

Journal Pre-proofs

Static analysis of FGM cylindrical shells and the effect of stress concentration using quasi-3D type higher-order shear deformation theory

Tran Ngoc Doan, Anh Tuan Nguyen, Phung Van Binh, Tran Van Hung, Vu Quoc Tru, Doan Trac Luat

PII: S0263-8223(20)33283-9
DOI: <https://doi.org/10.1016/j.compstruct.2020.113357>
Reference: COST 113357

To appear in: *Composite Structures*

Received Date: 17 May 2020
Accepted Date: 15 November 2020

Please cite this article as: Ngoc Doan, T., Tuan Nguyen, A., Van Binh, P., Van Hung, T., Quoc Tru, V., Trac Luat, D., Static analysis of FGM cylindrical shells and the effect of stress concentration using quasi-3D type higher-order shear deformation theory, *Composite Structures* (2020), doi: <https://doi.org/10.1016/j.compstruct.2020.113357>

This is a PDF file of an article that has undergone enhancements after acceptance, such as the addition of a cover page and metadata, and formatting for readability, but it is not yet the definitive version of record. This version will undergo additional copyediting, typesetting and review before it is published in its final form, but we are providing this version to give early visibility of the article. Please note that, during the production process, errors may be discovered which could affect the content, and all legal disclaimers that apply to the journal pertain.

© 2020 Published by Elsevier Ltd.



Static analysis of FGM cylindrical shells and the effect of stress concentration using quasi-3D type higher-order shear deformation theory

Tran Ngoc Doan^{1*}, Anh Tuan Nguyen¹, Phung Van Binh¹, Tran Van Hung¹, Vu Quoc Tru¹, Doan Trac Luat²

¹*Faculty of Aerospace Engineering, Le Quy Don Technical University, Hanoi City, Vietnam*

²*Faculty of Mechanical Engineering, Le Quy Don Technical University, Hanoi City, Vietnam*

*Corresponding author

Email: ngocdoanmai@gmail.com, tranngocdoan@lqdtu.edu.vn (T.N.Doan)

Abstract

This paper explores the stress concentration effect and the static responses of FGM cylindrical shells with various boundary conditions using the quasi-3D type higher-order shear deformation theory and the analytical approach. The displacement field is expressed by polynomials of the coordinate along the thickness direction. Compared to the polynomial used to analyze the transverse displacement, the order of the in-plane displacement polynomial is increased by one. The equations of equilibrium and their corresponding boundary conditions are derived based on the principle of virtual work. Using simple trigonometric series and the Laplace transform, the solutions of boundary problems with different conditions are derived. The results from the present theoretical models are compared with previously published data using several other models, including the 3D exact model. The paper also exhibits the effects of the boundary condition, the relative thickness, the relative length and the power-law index on the displacements and the stresses of shells. The stress concentration phenomenon is studied, and then the effects of several structural and material parameters on the concentrated stress are shown and assessed.

Keywords: Stress concentration effect; Analytical approach; FGM cylindrical shells; Quasi-3D type higher-order shear deformation theory; Elasticity.

1. Introduction

Due to the advanced characteristics compared to the conventional materials, such as high rigidity and strength, low weight and modest cost, composite materials have become popular for many applications in aerospace, mechanical, automobile and civil engineering. The most commonly observed drawback of composite materials is the inconsistency between their fibers and matrix in terms of mechanical properties. Hence, stress concentration may occur at the interface of these components, particularly in a high-temperature surrounding environment. This phenomenon may be the cause of several types of structural damage, such as delamination and cracks.

Functionally graded materials (FGMs) have been created to minimize the effect of the abovementioned disadvantage of composite materials. An FGM is regarded as an advanced composite material, which is manufactured from several components with the smooth variations of the mechanical properties between surfaces. Therefore, in an FGM, stress concentration does not occur. The concept of FGMs was introduced by Japanese researchers in 1984 [1]. Due to their practical applications, FGMs have grasped the attention of many researchers. The history of FGMs may be found in the literature [2] by Jha et al. The overview of mathematical models used in FGM structural analyses was presented by Birman and Byrd [3], and Thai and Kim [4]

Developing shell theories with a high accuracy level to model the responses of shell structures subjected to external loads has drawn the interest of many researchers in recent years. An increasing number of shell theories have been developed on the basis of various assumptions and approximation methods. Normally, researchers make simplification assumptions for thin shells and apply them to thicker ones, and at the same time, a 3D problem is converted to a 2D counterpart. We can categorize the shell theories into three groups: classical shell theory (CST), first-order shear deformation theory (FSDT) and higher-order shear deformation theory (HSDT). The overview of these shell theories can be found in the literature [5] of Reddy. The CST was developed originally for thin shells based on the Kirchhoff-Love kinematic hypothesis that the

straight lines normal to the undeformed reference surface remain straight and normal to the reference surface after deformation [6]. Using this assumption, the effect of transverse shear deformations is neglected. The CST is applicable to most shell problems, such as analyses of the responses of shells with or without elastic foundation due to thermal and mechanical loads [7-9], analyses of shell dynamics [10-12], and stability analyses [13-15], etc. To obtain more accurate results of shell dynamic responses with moderate thickness and overcome the weaknesses of the CST, the FSDT was introduced. The FSDT includes the effect of transverse shear deformation [16]. The FSDT can be used in classical problems, such as statically analyzing shell subjected to various loads [17-19], analyzing shell dynamics [20-23], analyzing shell stability [24-25], etc. In the FSDT, a shear correction factor is employed to obtain the transverse shear stiffness of a shell. However, the value of this factor is not a constant but rather dependent on several parameters including the material properties, the loading and the boundary conditions, etc. [5]. HSDTs were developed as an improvement of the FSDT in an effort to produce the more accurate results of the mechanical responses of shells. Several typical studies with HSDTs can be listed as Reddy and Liu [26], Touratier [27], Ferreira et al. [28], Carrera [29], Mantari et al. [30] and Viola et al. [31]. HSDTs are based on assumptions of the high-order variations of tangential displacement, or both tangential and transverse displacement components. Using HSDTs for shell structures usually provides closer results to the 3D elastic theory than those by the FSDT and CST.

The choice of the HSDT model used in a specific problem depends on the significance of each factor. Naghdi [32] developed a calculation model based on the analysis result of displacement along the thickness direction, in which tangential and transverse displacement components are expressed by first- and second-order polynomials, respectively. Reddy and Liu [26] introduced an HSDT while assuming that the variation of tangential displacement takes the form of a third-order polynomial, and transverse displacement is a constant. Using the free-boundary assumption, the number of independent displacement components is reduced to five. Vasilev and Lurie [33] analyzed the displacement field along the thickness direction together

with energy compatibility conditions to establish the fundamental equations and the boundary conditions for shallow shells. Based on the approach developed by Vasilev and Lurie, Doan et al. studied static and vibrating metal [34, 35] and laminated anisotropic [36] cylindrical shell. In these studies, the stress concentration phenomenon was investigated by a quasi-3D type HSDT model. Using an incomplete TSDT model, Neves et al. [37] conducted vibration analyses of FGM shells. A complete model based on the third-order polynomial of the displacement field was used by Punera and Kant for the static and free vibration analyses of FGM sandwich [38] and FGM open [39] cylindrical shells. Mantari and Guedes Soares [40] presented their analysis results of bending thick FGM shells using the trigonometric HSDT. Combining polynomial and trigonometric series to form a hybrid quasi-3D type HSDT model, Neves et al. [41] and Ferreira et al. [42] conducted static and free vibration analyses of FGM plates. From the above survey, it is seen that the previous studies using HSDT models have not focused on the stress concentration effect in FGM shell structures.

In this paper, several different quasi-3D type HSDT models, which are presented in [33-36], are employed to study FGM cylindrical shells. The fundamental equations and the boundary conditions are derived using the principle of virtual work. The solutions with various boundary conditions are obtained with the use of simple trigonometric series and the Laplace transform. The results in this paper are validated against those from an exact 3D model and several others. Compared to previous studies, in this work, the stress concentration phenomenon is analyzed intensively, and the effects of structural and material distribution parameters on the stress components in the regions of this phenomenon are assessed.

2. Theoretical formulation

In this paper, we consider an FGM cylindrical shell of length L , radius R and thickness h . An orthogonal curvilinear coordinate system $O\xi\theta z$, which is shown in Fig. 1, is employed. The neutral surface is assumed to coincide with the middle surface. The displacements of an arbitrary point of the shell in the ξ , θ and z directions are denoted by u , v and w ,

respectively. The Young's modulus E , Poisson's ratio μ are assumed to be functions of the volume fraction of constituent materials. The shell is subjected to transverse normal loads $q^+(\xi, \theta)$ and $q^-(\xi, \theta)$ on the outer and inner surfaces, respectively.

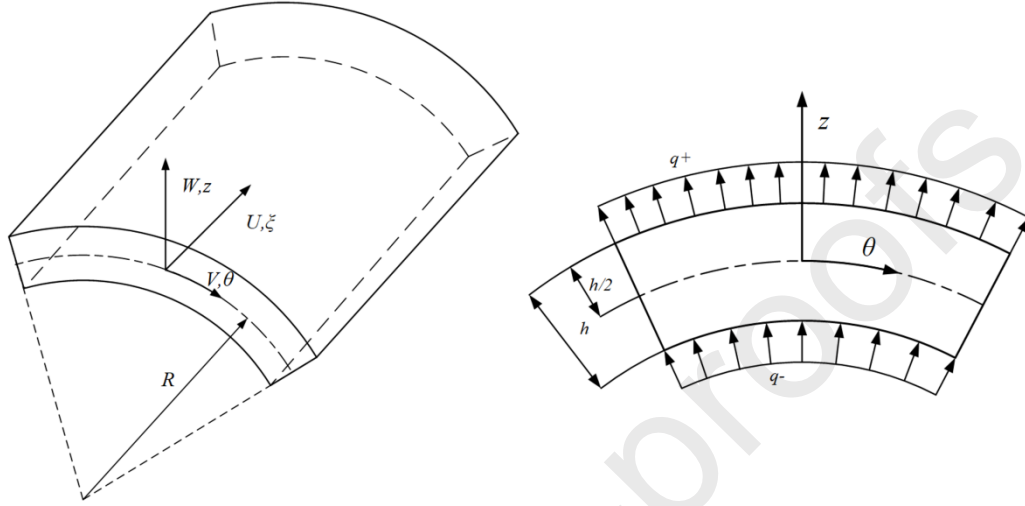


Fig. 1. Geometry and notations of a FGM cylindrical shell

2.1. Displacement fields and strains

The displacement field of the shell in the orthogonal curvilinear coordinate system $O\xi\theta z$ is expressed by

$$u(\xi, \theta, z) = \sum_{k=0}^K u_k(\xi, \theta) \frac{z^k}{k!}, \quad v(\xi, \theta, z) = \sum_{k=0}^K v_k(\xi, \theta) \frac{z^k}{k!}, \quad w(\xi, \theta, z) = \sum_{k=0}^{K-1} w_k(\xi, \theta) \frac{z^k}{k!}, \quad (1)$$

where u_0 , v_0 and w_0 are the 2D displacements of an arbitrary point in the ξ , θ and z directions, respectively. u_1 and v_1 are the transverse normal rotations corresponding to the ξ , θ axes. The other terms in equation (1) are the 2D high-order displacements according to the Taylor series.

The strain–displacements relations given by the linear part of Green-Lagrange strain tensor in the orthogonal curvilinear coordinate system $O\xi\theta z$ is defined as follows [5]:

$$\begin{aligned} \varepsilon_\xi &= \frac{1}{R} \frac{\partial u}{\partial \xi}, \quad \varepsilon_\theta = \frac{1}{R+z} \left(\frac{\partial v}{\partial \theta} + w \right), \quad \gamma_{\xi\theta} = \frac{1}{R} \frac{\partial v}{\partial \xi} + \frac{1}{R+z} \frac{\partial u}{\partial \theta}, \\ \gamma_{\theta z} &= \frac{1}{R+z} \frac{\partial w}{\partial \theta} + \frac{\partial v}{\partial z} - \frac{v}{R+z}, \quad \gamma_{\xi z} = \frac{1}{R} \frac{\partial w}{\partial \xi} + \frac{\partial u}{\partial z}, \quad \varepsilon_z = \frac{1}{R} \frac{\partial w}{\partial z}. \end{aligned} \quad (2)$$

Substituting the expressions of the displacement components in equation (1) into equation (2), we obtain the strain field as follows:

- For the displacement model with $K = 3$

$$\begin{aligned}\varepsilon_{\xi} &= \frac{1}{R} \left(\varepsilon_{\xi}^0 + \chi_{\xi z} z + \varepsilon_{\xi}^* \frac{z^2}{2} + \chi_{\xi}^* \frac{z^3}{3!} \right), \quad \varepsilon_{\theta} = \frac{1}{R+z} \left(\varepsilon_{\theta}^0 + \chi_{\theta z} z + \varepsilon_{\theta}^* \frac{z^2}{2} + \chi_{\theta}^* \frac{z^3}{3!} \right), \\ \gamma_{\xi\theta} &= \frac{1}{R} \left(\gamma_{\xi\theta}^0 + \chi_{\xi\theta z} z + \gamma_{\xi\theta}^* \frac{z^2}{2} + \chi_{\xi\theta}^* \frac{z^3}{3!} \right) + \frac{1}{R+z} \left(\lambda_{\theta\xi}^0 + \kappa_{\theta\xi} z + \lambda_{\theta\xi}^* \frac{z^2}{2} + \kappa_{\theta\xi}^* \frac{z^3}{3!} \right), \\ \gamma_{\xi z} &= \frac{1}{R} \left(\gamma_{\xi z}^0 + \chi_{\xi z} z + \gamma_{\xi z}^* \frac{z^2}{2} + \chi_{\xi z}^* \frac{z^3}{3!} \right), \quad \varepsilon_z = \frac{1}{R} (\varepsilon_z^0 + \chi_z z), \\ \gamma_{\theta z} &= \frac{1}{R+z} \left(\gamma_{\theta z}^0 + \chi_{\theta z} z + \gamma_{\theta z}^* \frac{z^2}{2} + \chi_{\theta z}^* \frac{z^3}{3!} \right),\end{aligned}\tag{3}$$

- For the displacement model with $K = 2$

$$\begin{aligned}\varepsilon_{\xi} &= \frac{1}{R} \left(\varepsilon_{\xi}^0 + \chi_{\xi z} z + \varepsilon_{\xi}^* \frac{z^2}{2} \right), \quad \varepsilon_{\theta} = \frac{1}{R+z} \left(\varepsilon_{\theta}^0 + \chi_{\theta z} z + \varepsilon_{\theta}^* \frac{z^2}{2} \right), \quad \varepsilon_z = \frac{1}{R} \varepsilon_z^0, \\ \gamma_{\xi\theta} &= \frac{1}{R} \left(\gamma_{\xi\theta}^0 + \chi_{\xi\theta z} z + \gamma_{\xi\theta}^* \frac{z^2}{2} \right) + \frac{1}{R+z} \left(\lambda_{\theta\xi}^0 + \kappa_{\theta\xi} z + \lambda_{\theta\xi}^* \frac{z^2}{2} \right), \\ \gamma_{\xi z} &= \frac{1}{R} \left(\gamma_{\xi z}^0 + \chi_{\xi z} z + \gamma_{\xi z}^* \frac{z^2}{2} \right), \quad \gamma_{\theta z} = \frac{1}{R+z} \left(\gamma_{\theta z}^0 + \chi_{\theta z} z + \gamma_{\theta z}^* \frac{z^2}{2} \right),\end{aligned}\tag{4}$$

where

$$\begin{aligned}\varepsilon_{\xi}^0 &= \frac{\partial u_0}{\partial \xi}, \quad \chi_{\xi} = \frac{\partial u_1}{\partial \xi}, \quad \varepsilon_{\xi}^* = \frac{\partial u_2}{\partial \xi}, \quad \chi_{\xi}^* = \frac{\partial u_3}{\partial \xi}, \quad \varepsilon_z^0 = w_1, \quad \chi_z = w_2, \quad \varepsilon_{\theta}^0 = \frac{\partial v_0}{\partial \theta} + w_0, \\ \chi_{\theta} &= \frac{\partial v_1}{\partial \theta} + w_1, \quad \varepsilon_{\theta}^* = \frac{\partial v_2}{\partial \theta} + w_2, \quad \chi_{\theta}^* = \frac{\partial v_3}{\partial \theta}, \quad \gamma_{\xi\theta}^0 = \frac{\partial v_0}{\partial \xi}, \quad \chi_{\xi\theta} = \frac{\partial v_1}{\partial \xi}, \\ \gamma_{\xi\theta}^* &= \frac{\partial v_2}{\partial \xi}, \quad \chi_{\xi\theta}^* = \frac{\partial v_3}{\partial \xi}, \quad \lambda_{\theta\xi}^0 = \frac{\partial u_0}{\partial \theta}, \quad \kappa_{\theta\xi} = \frac{\partial u_1}{\partial \theta}, \quad \lambda_{\theta\xi}^* = \frac{\partial u_2}{\partial \theta}, \quad \kappa_{\theta\xi}^* = \frac{\partial u_3}{\partial \theta}, \\ \gamma_{\xi z}^0 &= \frac{\partial w_0}{\partial \xi} + Ru_1, \quad \chi_{\xi z} = \frac{\partial w_1}{\partial \xi} + Ru_2, \quad \gamma_{\xi z}^* = \frac{\partial w_2}{\partial \xi} + Ru_3, \quad \chi_{\xi z}^* = 0, \\ \gamma_{\theta z}^0 &= \frac{\partial w_0}{\partial \theta} + Rv_1 - v_0, \quad \chi_{\theta z} = \frac{\partial w_1}{\partial \theta} + Rv_2, \quad \gamma_{\theta z}^* = \frac{\partial w_2}{\partial \theta} + Rv_3 + v_2, \quad \chi_{\theta z}^* = 2v_3.\end{aligned}\tag{5}$$

2.2. Constitutive relations

The material property gradation of a two-constituent FGM's in the thickness direction is involved in this study, and the following expression represents the profile of the volume fraction.

$$P_{FGM}(z) = (P_t - P_b)V + P_b, \quad (6)$$

where $V = \left(\frac{z}{h} + \frac{1}{2}\right)^\eta$; P_{FGM} denotes material parameters, such as the Young's modulus E and the Poisson's ratio μ ; P_t and P_b are the parameters at the top and bottom surfaces of the shell, respectively; and η is the power-law index that is a positive real number. The FGM material properties vary smoothly across the shell thickness. Material 1 is placed at the inner surface and material 2 is at the outer surface.

The 3D linear constitutive relations of a cylindrical shell are

$$\begin{Bmatrix} \sigma_\xi \\ \sigma_\theta \\ \sigma_z \\ \tau_{\xi\theta} \\ \tau_{\xi z} \\ \tau_{\theta z} \end{Bmatrix} = \begin{bmatrix} C_{11} & C_{12} & C_{13} & 0 & 0 & 0 \\ C_{21} & C_{22} & C_{23} & 0 & 0 & 0 \\ C_{31} & C_{32} & C_{33} & 0 & 0 & 0 \\ 0 & 0 & 0 & C_{44} & 0 & 0 \\ 0 & 0 & 0 & 0 & C_{55} & 0 \\ 0 & 0 & 0 & 0 & 0 & C_{66} \end{bmatrix} \begin{Bmatrix} \varepsilon_\xi \\ \varepsilon_\theta \\ \varepsilon_z \\ \gamma_{\xi\theta} \\ \gamma_{\xi z} \\ \gamma_{\theta z} \end{Bmatrix}, \quad (7)$$

where

$$C_{11} = C_{22} = C_{33} = \frac{E_{FGM}(1 - \mu_{FGM})}{(1 + \mu_{FGM})(1 - 2\mu_{FGM})}, \quad C_{44} = C_{55} = C_{66} = \frac{E_{FGM}}{2(1 + \mu_{FGM})},$$

$$C_{12} = C_{21} = C_{13} = C_{31} = C_{23} = C_{32} = \frac{E_{FGM}\mu_{FGM}}{(1 + \mu_{FGM})(1 - 2\mu_{FGM})}.$$

2.3. Governing equations

The governing equations are based on the equilibrium state and obtained by the use of the principle of virtual displacements. The principle of virtual work in the present case is given as

$$\begin{aligned} & \iiint_{\xi\theta z} (\sigma_\xi \delta\varepsilon_\xi + \sigma_\theta \delta\varepsilon_\theta + \sigma_z \delta\varepsilon_z + \tau_{\xi\theta} \delta\gamma_{\xi\theta} + \tau_{\xi z} \delta\gamma_{\xi z} + \tau_{\theta z} \delta\gamma_{\theta z}) R^2 \left(1 + \frac{z}{R}\right) d\xi d\theta dz - \\ & - \int \int_{\xi\theta} \left[q^+ \delta w^+ \left(1 + \frac{h}{2R}\right) + q^- \delta w^- \left(1 - \frac{h}{2R}\right) \right] R^2 d\xi d\theta = 0, \end{aligned} \quad (8)$$

in which $\delta w^+ = \delta w_0 + \frac{h}{2} \delta w_1 + \frac{h^2}{8} \delta w_2$, $\delta w^- = \delta w_0 - \frac{h}{2} \delta w_1 + \frac{h^2}{8} \delta w_2$.

Substituting equations (2) – (5) and (7) into equation (8) and integrating this equation through the thickness of the shell we derive:

- For the displacement model with $K = 3$

$$\begin{aligned} & \iint_{\xi\theta} \left(N_{\xi} \delta \varepsilon_{\xi}^0 + M_{\xi} \delta \chi_{\xi} + N_{\xi}^* \delta \varepsilon_{\xi}^* + M_{\xi}^* \delta \chi_{\xi}^* + N_{\theta} \delta \varepsilon_{\theta}^0 + M_{\theta} \delta \chi_{\theta} + N_{\theta}^* \delta \varepsilon_{\theta}^* + M_{\theta}^* \delta \chi_{\theta}^* + Q_z \delta \varepsilon_z^0 + \right. \\ & + S_z \delta \chi_z + N_{\xi\theta} \delta \gamma_{\xi\theta}^0 + M_{\xi\theta} \delta \chi_{\xi\theta} + N_{\xi\theta}^* \delta \gamma_{\xi\theta}^* + M_{\xi\theta}^* \delta \chi_{\xi\theta}^* + N_{\theta\xi} \delta \lambda_{\theta\xi}^0 + M_{\theta\xi} \delta \kappa_{\theta\xi} + N_{\theta\xi}^* \delta \lambda_{\theta\xi}^* + \\ & + M_{\theta\xi}^* \delta \kappa_{\theta\xi}^* + Q_{\xi} \delta \gamma_{\xi z}^0 + S_{\xi} \delta \chi_{\xi z} + Q_{\xi}^* \delta \gamma_{\xi z}^* + Q_{\theta} \delta \gamma_{\theta z}^0 + S_{\theta} \delta \chi_{\theta z} + Q_{\theta}^* \delta \gamma_{\theta z}^* + S_{\theta}^* \delta \chi_{\theta z}^* \left. \right) R d\xi d\theta - \\ & - \int \int_{\xi\theta} (p_0 \delta w_0 + p_1 \delta w_1 + p_2 \delta w_2) R^2 d\xi d\theta = 0, \end{aligned} \quad (9)$$

- For the displacement model with $K = 2$

$$\begin{aligned} & \iint_{\xi\theta} \left(N_{\xi} \delta \varepsilon_{\xi}^0 + M_{\xi} \delta \chi_{\xi} + N_{\xi}^* \delta \varepsilon_{\xi}^* + N_{\theta} \delta \varepsilon_{\theta}^0 + M_{\theta} \delta \chi_{\theta} + N_{\theta}^* \delta \varepsilon_{\theta}^* + Q_z \delta \varepsilon_z^0 + N_{\xi\theta} \delta \gamma_{\xi\theta}^0 + \right. \\ & + M_{\xi\theta} \delta \chi_{\xi\theta} + N_{\xi\theta}^* \delta \gamma_{\xi\theta}^* + N_{\theta\xi} \delta \lambda_{\theta\xi}^0 + M_{\theta\xi} \delta \kappa_{\theta\xi} + N_{\theta\xi}^* \delta \lambda_{\theta\xi}^* + Q_{\xi} \delta \gamma_{\xi z}^0 + S_{\xi} \delta \chi_{\xi z} + \\ & + Q_{\theta} \delta \gamma_{\theta z}^0 + S_{\theta} \delta \chi_{\theta z} + Q_{\theta}^* \delta \gamma_{\theta z}^* \left. \right) R d\xi d\theta - \int \int_{\xi\theta} (p_0 \delta w_0 + p_1 \delta w_1) R^2 d\xi d\theta = 0, \end{aligned} \quad (10)$$

where

$$\begin{aligned} (N_{\xi}, M_{\xi}, N_{\xi}^*, M_{\xi}^*) &= \int_{-h/2}^{+h/2} \sigma_{\xi} \left(1 + \frac{z}{R} \right) \left(1, z, \frac{z^2}{2}, \frac{z^3}{6} \right) dz, \\ (N_{\theta}, M_{\theta}, N_{\theta}^*, M_{\theta}^*) &= \int_{-h/2}^{+h/2} \sigma_{\theta} \left(1, z, \frac{z^2}{2}, \frac{z^3}{6} \right) dz, \quad (Q_z, S_z) = \int_{-h}^{+h} \sigma_z (1, z) \left(1 + \frac{z}{R} \right) dz, \\ (N_{\theta\xi}, M_{\theta\xi}, N_{\theta\xi}^*, M_{\theta\xi}^*) &= \int_{-h/2}^{+h/2} \tau_{\theta\xi} \left(1, z, \frac{z^2}{2}, \frac{z^3}{6} \right) dz, \\ (N_{\xi\theta}, M_{\xi\theta}, N_{\xi\theta}^*, M_{\xi\theta}^*) &= \int_{-h/2}^{+h/2} \tau_{\xi\theta} \left(1 + \frac{z}{R} \right) \left(1, z, \frac{z^2}{2}, \frac{z^3}{6} \right) dz, \\ (Q_{\xi}, S_{\xi}, Q_{\xi}^*) &= \int_{-h/2}^{+h/2} \tau_{\xi z} \left(1, z, \frac{z^2}{2} \right) \left(1 + \frac{z}{R} \right) dz, \\ (Q_{\theta}, S_{\theta}, Q_{\theta}^*, S_{\theta}^*) &= \int_{-h/2}^{+h/2} \tau_{\theta z} \left(1, z, \frac{z^2}{2}, \frac{z^3}{6} \right) dz, \end{aligned} \quad (11)$$

$$p_i = q^+ \left(1 + \frac{h}{2R}\right) \frac{(h/2)^i}{i!} + q^- \left(1 - \frac{h}{2R}\right) \frac{(-h/2)^i}{i!}, \quad i = 0, 1, 2.$$

The equations of equilibrium can be derived from equations (9) and (10) by integrating the displacement gradients by parts and setting the coefficients δu_k , δv_k and δw_k to zero separately.

Thus, one can obtain the equilibrium equations associated with the present quasi-3D type HSDT:

$$\begin{aligned} \delta u_0 : \frac{\partial N_\xi}{\partial \xi} + \frac{\partial N_{\theta\xi}}{\partial \theta} &= 0, \\ \delta v_0 : \frac{\partial N_\theta}{\partial \theta} + \frac{\partial N_{\xi\theta}}{\partial \xi} + Q_\theta &= 0, \\ \delta w_0 : \frac{\partial Q_\xi}{\partial \xi} + \frac{\partial Q_\theta}{\partial \theta} - N_\theta - Rp_0 &= 0, \\ \delta u_1 : \frac{\partial M_\xi}{\partial \xi} + \frac{\partial M_{\theta\xi}}{\partial \theta} - RQ_\xi &= 0, \\ \delta v_1 : \frac{\partial M_{\xi\theta}}{\partial \xi} + \frac{\partial M_\theta}{\partial \theta} - RQ_\theta &= 0, \\ \delta w_1 : \frac{\partial S_\xi}{\partial \xi} + \frac{\partial S_\theta}{\partial \theta} - M_\theta - RQ_z - Rp_1 &= 0, \\ \delta u_2 : \frac{\partial N_\xi^*}{\partial \xi} + \frac{\partial N_{\theta\xi}^*}{\partial \theta} - RS_\xi &= 0, \\ \delta v_2 : \frac{\partial N_{\xi\theta}^*}{\partial \xi} + \frac{\partial N_\theta^*}{\partial \theta} - RS_\theta - Q_\theta^* &= 0, \\ \delta w_2 : \frac{\partial Q_\xi^*}{\partial \xi} + \frac{\partial Q_\theta^*}{\partial \theta} - N_\theta^* - RS_z - Rp_2 &= 0, \\ \delta u_3 : \frac{\partial M_\xi^*}{\partial \xi} + \frac{\partial M_{\theta\xi}^*}{\partial \theta} - RQ_\xi^* &= 0, \\ \delta v_3 : \frac{\partial M_{\xi\theta}^*}{\partial \xi} + \frac{\partial M_\theta^*}{\partial \theta} - RQ_\theta^* - 2S_\theta^* &= 0. \end{aligned} \tag{12}$$

The boundary condition of equation (11) may take one of the following forms:

- For the boundary condition $\xi = const$

$$\begin{aligned}
 N_{\xi} &= \bar{N}_{\xi} \cup u_0 = \bar{u}_0, \quad N_{\xi\theta} = \bar{N}_{\xi\theta} \cup v_0 = \bar{v}_0, \quad Q_{\xi} = \bar{Q}_{\xi} \cup w_0 = \bar{w}_0, \\
 M_{\xi} &= \bar{M}_{\xi} \cup u_1 = \bar{u}_1, \quad M_{\xi\theta} = \bar{M}_{\xi\theta} \cup v_1 = \bar{v}_1, \quad S_{\xi} = \bar{S}_{\xi} \cup w_1 = \bar{w}_1, \\
 N_{\xi}^* &= \bar{N}_{\xi}^* \cup u_2 = \bar{u}_2, \quad N_{\xi\theta}^* = \bar{N}_{\xi\theta}^* \cup v_2 = \bar{v}_2, \quad Q_{\xi}^* = \bar{Q}_{\xi}^* \cup w_2 = \bar{w}_2, \\
 M_{\xi}^* &= \bar{M}_{\xi}^* \cup u_3 = \bar{u}_3, \quad M_{\xi\theta}^* = \bar{M}_{\xi\theta}^* \cup v_3 = \bar{v}_3,
 \end{aligned} \tag{13}$$

- For the boundary condition $\theta = const$

$$\begin{aligned}
 N_{\theta\xi} &= \bar{N}_{\theta\xi} \cup u_0 = \bar{u}_0, \quad N_{\theta} = \bar{N}_{\theta} \cup v_0 = \bar{v}_0, \quad Q_{\theta} = \bar{Q}_{\theta} \cup w_0 = \bar{w}_0, \\
 M_{\theta\xi} &= \bar{M}_{\theta\xi} \cup u_0 = \bar{u}_0, \quad M_{\theta} = \bar{M}_{\theta} \cup v_1 = \bar{v}_1, \quad S_{\theta} = \bar{S}_{\theta} \cup w_1 = \bar{w}_1, \\
 N_{\theta\xi}^* &= \bar{N}_{\theta\xi}^* \cup u_2 = \bar{u}_2, \quad N_{\theta}^* = \bar{N}_{\theta}^* \cup v_2 = \bar{v}_2, \quad Q_{\theta}^* = \bar{Q}_{\theta}^* \cup w_2 = \bar{w}_2, \\
 M_{\theta\xi}^* &= \bar{M}_{\theta\xi}^* \cup u_3 = \bar{u}_3, \quad M_{\theta}^* = \bar{M}_{\theta}^* \cup v_3 = \bar{v}_3.
 \end{aligned} \tag{14}$$

Equations (13) and (14) cover all types of boundary condition, and the number of the boundary conditions equals to the order of the differential equation system.

In the case of a closed cylindrical shell, the boundary condition presented in equation (14) is replaced by a periodic condition with respect to the θ coordinate. The boundary condition in equation (13) can be simplified for some common cases as

- For fully clamped boundary condition:

$$u_0 = u_1 = u_2 = u_3 = 0, \quad v_0 = v_1 = v_2 = v_3 = 0, \quad w_0 = w_1 = w_2 = 0, \tag{15}$$

- For fully simply supported boundary condition:

$$N_{\xi} = M_{\xi} = N_{\xi}^* = M_{\xi}^* = 0, \quad v_0 = v_1 = v_2 = v_3 = 0, \quad w_0 = w_1 = w_2 = 0. \tag{16}$$

- For fully free boundary condition:

$$N_{\xi} = M_{\xi} = N_{\xi}^* = M_{\xi}^* = 0, \quad N_{\xi\theta} = M_{\xi\theta} = N_{\xi\theta}^* = M_{\xi\theta}^* = 0, \quad Q_{\xi} = S_{\xi} = Q_{\xi}^* = 0, \tag{17}$$

3. Solving process

3.1. Converting partial differential equations to ordinary differential equations

The equilibrium equation (12) gives us the system of $3K + 2$ differential equations for $3K + 2$ displacement components u_k, v_k, w_k and the number of degrees of freedom is $2(3K + 2)$. Equation (12) is re-written as

$$\begin{aligned}
 & \sum_{i=0}^K \left(H_{1i}^l + H_{1i,11}^l \frac{\partial^2}{\partial \xi^2} + H_{1i,22}^l \frac{\partial^2}{\partial \theta^2} \right) u_i + \sum_{i=0}^K H_{2i,12}^l \frac{\partial^2}{\partial \xi \partial \theta} v_i + \\
 & \quad + \sum_{i=0}^{K-1} H_{3i,1}^l \frac{\partial}{\partial \xi} w_i = 0, \quad l = 1, \dots, (K + 1), \\
 & \sum_{i=0}^K H_{1i,12}^k \frac{\partial^2}{\partial \xi \partial \theta} u_i + \sum_{i=0}^K \left(H_{2i}^k + H_{2i,11}^k \frac{\partial^2}{\partial \xi^2} + H_{2i,22}^k \frac{\partial^2}{\partial \theta^2} \right) v_i + \\
 & \quad + \sum_{i=0}^{K-1} H_{3i,2}^k \frac{\partial}{\partial \theta} w_i = 0, \quad k = (K + 2), \dots, (2K + 2), \\
 & \sum_{i=0}^K H_{1i,1}^n \frac{\partial}{\partial \xi} u_i + \sum_{i=0}^{K-1} \left(H_{3i}^n + H_{3i,11}^n \frac{\partial^2}{\partial \xi^2} + H_{3i,22}^n \frac{\partial^2}{\partial \theta^2} \right) w_i + \\
 & \quad + \sum_{i=0}^K H_{2i,2}^n \frac{\partial}{\partial \theta} v_i = H_{q^+}^n q^+ - H_{q^-}^n q^-, \quad n = (2K + 3), \dots, (3K + 2),
 \end{aligned} \tag{18}$$

herein, the coefficients H are constants, which depend on the radius R , the relative thickness h/R , Poisson's ratio μ_{FGM} , and Young's modulus E_{FGM} of the whole structure. These constants are determined by synchronizing the coefficients of the two equations (12) and (18).

We transform partial differential equations (18) into a system of ordinary differential equations. For a closed circular cylindrical shell, we employ an expansion method using trigonometric series with respect to the circumferential variable θ . The periodicity conditions are automatically satisfied. The displacement field and the load are represented by single trigonometric series as follows:

$$\begin{aligned}
 u_i(\xi, \theta) &= U_{i0}(\xi) + \sum_{m=1}^{\infty} \left[U_{im}^1(\xi) \cos m\theta + U_{im}^2(\xi) \sin m\theta \right], \\
 v_i(\xi, \theta) &= V_{i0}(\xi) + \sum_{m=1}^{\infty} \left[V_{im}^1(\xi) \sin m\theta - V_{im}^2(\xi) \cos m\theta \right],
 \end{aligned}$$

$$w_j(\xi, \theta) = W_{j_0}(\xi) + \sum_{m=1}^{\infty} [W_{jm}^1(\xi) \cos m\theta + W_{jm}^2(\xi) \sin m\theta], \quad (19)$$

$$q^\pm(\xi, \theta) = Q_0^\pm(\xi) + \sum_{m=1}^{\infty} [Q_m^{1\pm}(\xi) \cos m\theta + Q_m^{2\pm}(\xi) \sin m\theta],$$

$$i = 0, 1, \dots, K, \quad j = 0, 1, \dots, K-1.$$

Substituting equation (19) into equation (18) and performing some simple mathematical transformations, we can obtain differential equations to determine $U_{i_0}(\xi)$, $W_{j_0}(\xi)$ functions as

$$\begin{aligned} \sum_{i=0}^K \left(H_{1i}^l + H_{1i,11}^l \frac{d^2}{d\xi^2} \right) U_{i_0} + \sum_{i=0}^{K-1} H_{3i,1}^l \frac{dW_{j_0}}{d\xi} = 0, \quad l = 1, \dots, (K+1), \\ \sum_{i=0}^K H_{1i,1}^n \frac{dU_{i_0}}{d\xi} + \sum_{i=0}^{K-1} \left(H_{3i}^n + H_{3i,11}^n \frac{d^2}{d\xi^2} \right) W_{j_0} = H_{q^+}^n Q_0^+ - H_{q^-}^n Q_0^-, \quad n = (2K+3), \dots, (3K+2). \end{aligned} \quad (20)$$

In the case of symmetrical axial loading, the components $V_{i_0}(\xi) = 0$.

To determine functions $U_{im}^1(\xi)$, $V_{im}^1(\xi)$, $W_{jm}^1(\xi)$ and $U_{im}^2(\xi)$, $V_{im}^2(\xi)$, $W_{jm}^2(\xi)$, we obtain the system of differential equations in the same form as follows:

$$\begin{aligned} \sum_{i=0}^K \left(H_{1i}^l + H_{1i,11}^l \frac{d^2}{d\xi^2} - m^2 H_{1i,22}^l \right) U_{im} + m \sum_{i=0}^K H_{2i,12}^l \frac{d}{d\xi} V_{im} + \\ + \sum_{i=0}^{K-1} H_{3i,1}^l \frac{d}{d\xi} W_{im} = 0, \quad l = 1, \dots, (K+1), \\ -m \sum_{i=0}^K H_{1i,12}^k \frac{d}{d\xi} U_{im} + \sum_{i=0}^K \left(H_{2i}^k + H_{2i,11}^k \frac{d^2}{d\xi^2} - m^2 H_{2i,22}^k \right) V_{im} - \\ - m \sum_{i=0}^{K-1} H_{3i,2}^k W_{im} = 0, \quad k = (K+2), \dots, (2K+2), \\ \sum_{i=0}^K H_{1i,1}^n \frac{d}{d\xi} U_{im} + \sum_{i=0}^{K-1} \left(H_{3i}^n + H_{3i,11}^n \frac{d^2}{d\xi^2} - m^2 H_{3i,22}^n \right) W_{im} + \\ + m \sum_{i=0}^K H_{2i,2}^n V_{im} = H_{q^+}^n Q_m^+ - H_{q^-}^n Q_m^-, \quad n = (2K+3), \dots, (3K+2). \end{aligned} \quad (21)$$

In equation (21), we neglect the superscripts 1 and 2 of the quantities $U_{im}(\xi)$, $V_{im}(\xi)$ and $W_{jm}(\xi)$.

3.2. Solving boundary problems by the Laplace transform

The solutions from equations (20) and (21) are obtained using the Laplace transform. Equation (20) is regarded as a specific case of equation (21) when $m = 0$. Here, we study the solution from equation (21).

Let $\tilde{U}_{im}(p)$, $\tilde{V}_{im}(p)$ và $\tilde{W}_{jm}(p)$ be the image functions of $U_{im}(\xi)$, $V_{im}(\xi)$, $W_{jm}(\xi)$, respectively.

According to the rule of differentiating source functions, we derive:

$$\begin{aligned} \frac{d}{d\xi}U_{im}(\xi) &\doteq p\tilde{U}_{im}(p) - C_{im}^{10}, \quad \frac{d^2}{d\xi^2}U_{im}(\xi) \doteq p^2\tilde{U}_{im}(p) - pC_{im}^{10} - C_{im}^{11}, \\ \frac{d}{d\xi}V_{im}(\xi) &\doteq p\tilde{V}_{im}(p) - C_{im}^{20}, \quad \frac{d^2}{d\xi^2}V_{im}(\xi) \doteq p^2\tilde{V}_{im}(p) - pC_{im}^{20} - C_{im}^{21}, \\ \frac{d}{d\xi}W_{jm}(\xi) &\doteq p\tilde{W}_{jm}(p) - C_{jm}^{30}, \quad \frac{d^2}{d\xi^2}W_{jm}(\xi) \doteq p^2\tilde{W}_{jm}(p) - pC_{im}^{30} - C_{im}^{31}. \end{aligned} \quad (22)$$

where

$$\begin{aligned} C_{im}^{10} &= U_{im}(0), \quad C_{im}^{20} = V_{im}(0), \quad C_{jm}^{30} = W_{jm}(0), \\ C_{im}^{11} &= \left. \frac{d}{d\xi}U_{im}(\xi) \right|_{\xi=0}, \quad C_{im}^{21} = \left. \frac{d}{d\xi}V_{im}(\xi) \right|_{\xi=0}, \quad C_{jm}^{31} = \left. \frac{d}{d\xi}W_{jm}(\xi) \right|_{\xi=0}. \end{aligned} \quad (23)$$

Applying the Laplace transform to equation (21) and using equation (22), we derive the following algebraic equation with respect to $\tilde{U}_{im}(p)$, $\tilde{V}_{im}(p)$, $\tilde{W}_{jm}(p)$:

$$\begin{aligned} \sum_{i=0}^K (H_{1i}^l + H_{1i,11}^l p^2 - m^2 H_{1i,22}^l) \tilde{U}_{im}(p) + m \sum_{i=0}^K H_{2i,12}^l p \tilde{V}_{im}(p) + \sum_{i=0}^{K-1} H_{3i,1}^l p \tilde{W}_{im}(p) &= \\ = \sum_{i=0}^K H_{1i,11}^l (pC_{im}^{10} + C_{im}^{11}) + m \sum_{i=0}^K H_{2i,12}^l C_{im}^{20} + \sum_{i=0}^{K-1} H_{3i,1}^l C_{jm}^{30}, \quad l = 1, \dots, (K+1), \\ -m \sum_{i=0}^K H_{1i,12}^k p \tilde{U}_{im}(p) + \sum_{i=0}^K (H_{2i}^k + H_{2i,11}^k p^2 - m^2 H_{2i,22}^k) \tilde{V}_{im}(p) - m \sum_{i=0}^{K-1} H_{3i,2}^k \tilde{W}_{im}(p) &= \\ = -m \sum_{i=0}^K H_{1i,12}^k C_{im}^{10} + \sum_{i=0}^K H_{2i,11}^k (pC_{im}^{20} + C_{im}^{21}), \quad k = (K+2), \dots, (2K+2), \end{aligned} \quad (24)$$

$$\begin{aligned} & \sum_{i=0}^K H_{1i,1}^n p \tilde{U}_{im}(p) + \sum_{i=0}^{K-1} (H_{3i}^n + H_{3i,11}^n p^2 - m^2 H_{3i,22}^n) \tilde{W}_{im}(p) + m \sum_{i=0}^K H_{2i,2}^n \tilde{V}_{im}(p) = \\ & = H_{q^+}^n \tilde{Q}_m^+(p) - H_{q^-}^n \tilde{Q}_m^-(p) + \sum_{i=0}^K H_{1i,1}^n C_{im}^{10} + \sum_{i=0}^{K-1} H_{3i,11}^n (p C_{im}^{30} + C_{im}^{31}), \quad n = (2K+3), \dots, (3K+2). \end{aligned}$$

In equation (24), $\tilde{Q}_m^+(p)$, $\tilde{Q}_m^-(p)$ are respectively the image functions of $Q_m^+(\xi)$ and $Q_m^-(\xi)$.

For closed circular shells, the boundary conditions (15), (16) and (17) at $\xi = 0$ are analyzed through the constants of integration C_{im}^{10} , C_{im}^{20} , C_{jm}^{30} , C_{im}^{11} , C_{im}^{21} , C_{jm}^{31} , $i = 0, 1, \dots, K$, $j = 0, 1, \dots, (K-1)$ as follows:

- For the clamped boundary condition [equation (15)]:

$$C_{im}^{10} = 0, \quad C_{im}^{20} = 0, \quad C_{jm}^{30} = 0, \quad i = 0, 1, \dots, K, \quad j = 0, 1, \dots, (K-1). \quad (25)$$

- For the simply supported boundary condition [equation (16)]:

$$C_{im}^{11} = 0, \quad C_{im}^{20} = 0, \quad C_{jm}^{30} = 0, \quad i = 0, 1, \dots, K, \quad j = 0, 1, \dots, (K-1). \quad (26)$$

- The free boundary condition [equation (17)] can be rewritten in a form of a system of algebraic equations with respect to the constants of integration C_{im}^{10} , C_{im}^{20} , C_{jm}^{30} , C_{im}^{11} , C_{im}^{21} , C_{jm}^{31} , $i = 0, 1, \dots, K$, $j = 0, 1, \dots, (K-1)$:

$$N_{\xi} = 0: \quad \sum_{i=0}^K G_{1i}^1 C_{im}^{11} + m \sum_{i=0}^K G_{2i}^1 C_{im}^{20} + \sum_{j=0}^{K-1} G_{3j}^1 C_{jm}^{30} = 0,$$

$$M_{\xi} = 0: \quad \sum_{i=0}^K G_{1i}^2 C_{im}^{11} + m \sum_{i=0}^K G_{2i}^2 C_{im}^{20} + \sum_{j=0}^{K-1} G_{3j}^2 C_{jm}^{30} = 0,$$

$$N_{\xi}^* = 0: \quad \sum_{i=0}^K G_{1i}^3 C_{im}^{11} + m \sum_{i=0}^K G_{2i}^3 C_{im}^{20} + \sum_{j=0}^{K-1} G_{3j}^3 C_{jm}^{30} = 0,$$

$$M_{\xi}^* = 0: \quad \sum_{i=0}^K G_{1i}^4 C_{im}^{11} + m \sum_{i=0}^K G_{2i}^4 C_{im}^{20} + \sum_{j=0}^{K-1} G_{3j}^4 C_{jm}^{30} = 0,$$

$$N_{\xi\theta} = 0: \quad -m \sum_{i=0}^K G_{1i}^5 C_{im}^{10} + \sum_{i=0}^K G_{2i}^5 C_{im}^{21} = 0,$$

$$M_{\xi\theta} = 0: -m \sum_{i=0}^K G_{1i}^6 C_{im}^{10} + \sum_{i=0}^K G_{2i}^6 C_{im}^{21} = 0, \quad (27)$$

$$N_{\xi\theta}^* = 0: -m \sum_{i=0}^K G_{1i}^7 C_{im}^{10} + \sum_{i=0}^K G_{2i}^7 C_{im}^{21} = 0,$$

$$M_{\xi\theta}^* = 0: -m \sum_{i=0}^K G_{1i}^8 C_{im}^{10} + \sum_{i=0}^K G_{2i}^8 C_{im}^{21} = 0,$$

$$Q_{\xi} = 0: \sum_{i=0}^K G_{1i}^9 C_{im}^{11} + m \sum_{i=0}^K G_{2i}^9 C_{im}^{20} + \sum_{j=0}^{K-1} G_{3j}^9 C_{jm}^{30} = 0,$$

$$S_{\xi} = 0: \sum_{i=0}^K G_{1i}^{10} C_{im}^{11} + m \sum_{i=0}^K G_{2i}^{10} C_{im}^{20} + \sum_{j=0}^{K-1} G_{3j}^{10} C_{jm}^{30} = 0,$$

$$Q_{\xi}^* = 0: \sum_{i=0}^K G_{1i}^{11} C_{im}^{11} + m \sum_{i=0}^K G_{2i}^{11} C_{im}^{20} + \sum_{j=0}^{K-1} G_{3j}^{11} C_{jm}^{30} = 0.$$

Coefficients G_{1i}^n , G_{2i}^n , G_{3j}^n in equation (27) are obtained from the expressions of the generalized internal forces corresponding to equation (11). Let the values of C_{im}^{10} , C_{im}^{20} , C_{jm}^{30} be given, the system of equations (27) becomes linear with variables C_{im}^{11} , C_{im}^{21} , C_{jm}^{31} . Solving the system of algebraic equations (27), we can derive the expressions to determine C_{im}^{11} , C_{im}^{21} , C_{jm}^{31} through C_{im}^{10} , C_{im}^{20} , C_{jm}^{30} .

For example, for a homogeneous shell in the case of $K=3$, C_{im}^{11} , C_{im}^{21} , C_{jm}^{31} are expressed through C_{im}^{10} , C_{im}^{20} , C_{jm}^{30} as

$$\begin{aligned}
C_{0m}^{11} &= -\frac{\mu}{(1-\mu)}(C_{0m}^{30} + RC_{1m}^{30} + mC_{0m}^{20}), \\
C_{1m}^{11} &= \frac{\mu}{R(1-\mu)}(mC_{0m}^{20} + C_{0m}^{30} - mRC_{1m}^{20} - RC_{1m}^{30} - R^2C_{2m}^{30}), \\
C_{2m}^{11} &= -\frac{\mu}{R^2(1-\mu)}(2C_{0m}^{30} + 2mC_{0m}^{20} - 2RC_{1m}^{30} - 2mRC_{1m}^{20} + R^2C_{2m}^{30} + mR^2C_{2m}^{20}), \\
C_{3m}^{11} &= \frac{\mu}{R^3(1-\mu)}(6C_{0m}^{30} + 6mC_{0m}^{20} - 6RC_{1m}^{30} - 6mRC_{1m}^{20} + 3R^2C_{2m}^{30} + 3mR^2C_{2m}^{20} - mR^3C_{3m}^{20}), \\
C_{0m}^{21} &= mC_{0m}^{10}, \quad C_{1m}^{21} = m(C_{1m}^{10} - C_{0m}^{10}/R), \quad C_{2m}^{21} = m(2C_{0m}^{10} - 2RC_{1m}^{10} + R^2C_{2m}^{10})/R^2, \\
C_{3m}^{21} &= m(-6C_{0m}^{10} + 6RC_{1m}^{10} - 3R^2C_{2m}^{10} + R^3C_{3m}^{10})/R^3, \\
C_{0m}^{31} &= -RC_{1m}^{10}, \quad C_{1m}^{31} = -RC_{2m}^{10}, \quad C_{2m}^{31} = -RC_{3m}^{10}.
\end{aligned}$$

In the case of $K=2$, we can derive:

$$\begin{aligned}
C_{0m}^{11} &= -\frac{\mu}{(1-\mu)}(C_{0m}^{30} + RC_{1m}^{30} + mC_{0m}^{20}), \quad C_{1m}^{11} = \frac{\mu}{R(1-\mu)}(mC_{0m}^{20} + C_{0m}^{30} - mRC_{1m}^{20} - RC_{1m}^{30}), \\
C_{2m}^{11} &= -\frac{\mu}{R^2(1-\mu)}(2C_{0m}^{30} + 2mC_{0m}^{20} - 2RC_{1m}^{30} - 2mRC_{1m}^{20} + mR^2C_{2m}^{20}), \\
C_{0m}^{21} &= mC_{0m}^{10}, \quad C_{1m}^{21} = m(C_{1m}^{10} - C_{0m}^{10}/R), \quad C_{2m}^{21} = m(2C_{0m}^{10} + R^2C_{2m}^{10})/R^2, \\
C_{0m}^{31} &= -RC_{1m}^{10}, \quad C_{1m}^{31} = -RC_{2m}^{10}.
\end{aligned}$$

Therefore, through equations (25), (26) and (27), the boundary condition at an edge of the shell is automatically satisfied when we provide C_{im}^{10} , C_{im}^{20} , C_{jm}^{30} , C_{im}^{11} , C_{im}^{21} , C_{jm}^{31} with reasonable values. At the same time, half of the constants of integration are satisfied automatically; and thus, the solving process of equation (21) is simplified.

Solving the algebraic equation (24) while considering the boundary condition at $\xi = 0$ for the image functions $\tilde{U}_{im}(p)$, $\tilde{V}_{im}(p)$ and $\tilde{W}_{jm}(p)$, we derive the expressions of the image functions in a form of an algebraic fraction, whose numerator and denominator are polynomials of p . The inverse Laplace transform is applied to these functions to obtain the displacement components $U_{im}(\xi)$, $V_{im}(\xi)$ and $W_{jm}(\xi)$. The second half of constants of integration (23) are determined by the remaining boundary condition.

Substituting the derived expressions of $U_{im}(\xi)$, $V_{im}(\xi)$ and $W_{jm}(\xi)$ into equation (19), we can obtain the displacements components $u_i(\xi, \theta)$, $v_i(\xi, \theta)$ and $w_j(\xi, \theta)$. From equations (1), (2), (3), (4) and (5), we can derive the expressions of the deformation field. σ_ξ , σ_θ and $\tau_{\xi\theta}$ may be obtained from equation (9). The shear stress components are calculated by integrating the equation of equilibrium according to the 3D theory of elasticity as bellows:

$$\begin{aligned}\tau_{\xi z} &= -\frac{1}{R+z} \int_{-h/2}^z \left[\left(1 + \frac{z}{R}\right) \frac{\partial \sigma_\xi}{\partial \xi} + \frac{\partial \tau_{\xi\theta}}{\partial \theta} \right] dz, \\ \tau_{\theta z} &= -\frac{R}{(R+z)^2} \int_{-h/2}^z \left[\left(1 + \frac{z}{R}\right) \frac{\partial \sigma_\theta}{\partial \theta} + \left(1 + \frac{z}{R}\right)^2 \frac{\partial \tau_{\xi\theta}}{\partial \xi} \right] dz, \\ \sigma_z &= -\frac{1}{R+z} \int_{-h/2}^z \left[\left(1 + \frac{z}{R}\right) \frac{\partial \tau_{\xi z}}{\partial \xi} + \frac{\partial \tau_{\theta z}}{\partial \theta} - \sigma_\theta \right] dz + \frac{R-h/2}{R+h/2} q^-\end{aligned}$$

4. Numerical analysis and discussion

4.1. Validations

For the first validation analysis, we analyze an FGM cylindrical shell with both edges clamped. The input parameters are given in the literature [43] by Santos et al., which are the length $L = 0.381$ m, the radius $R = 0.1905$ m and the thickness $h = 0,000501$ m; the inner surface is made of Zirconia with $\mu_c = 0.2980$ and $E_c = 168.06$ GPa while the material of outer surface is stainless steel with $\mu_m = 0.3178$ and $E_m = 207.79$ GPa; the shell is subjected to outer pressure $q^+ = 1000$ Pa. Table 1 presents the transverse displacement w at the middle position of the shell for two theoretical models corresponding to $K=2$ and $K=3$. To validate the results, we make comparison with those from semi-analytical finite element models with the number of elements increasing from 60 to 120 [43].

Table 1

The transverse displacement $\bar{w} = w \times 10^7$ of the FGM cylindrical shell at the middle position.

η	60 Elements	90 Elements	120 Elements	Present	Present
--------	-------------	-------------	--------------	---------	---------

	[43]	[43]	[43]	$K=2$	$K=3$
10	-3.864	-3.859	-3.857	-3.857	-3.856
5	-3.794	-3.789	-3.787	-3.787	-3.786
1	-3.511	-3.506	-3.504	-3.504	-3.504
1/4	-3.289	-3.284	-3.282	-3.282	-3.282
1/6	-3.249	-3.244	-3.243	-3.243	-3.243
1/8	-3.228	-3.223	-3.221	-3.221	-3.221

When analyzing the data shown in Table 1, it is observed that the models corresponding to $K=2$ and $K=3$ presented in this paper can produce accurate results that are in good agreement with those from the semi-analytical finite element model using 120 elements. This agreement is sufficient to ascertain the validity of the present calculation model.

For the second validation analysis, we study an FGM cylindrical panel with the simply-supported edges. The input parameters are from the literature [44] by Brischetto, including the radius $R=10m$, the length $L=1m$, the arc length $b=\frac{\pi}{3}R$ and the relative thickness R/h is variable; the inner surface is made of Aluminum Alloy Al2024 with $\mu_m=0.3$ and $E_m=73GPa$ while the material of the outer surface is Alumina Al_2O_3 with $\mu_c=0.3$ and $E_c=380GPa$. The shell is subjected to a harmonic transverse normal load distributed on the outer surface $q^+ = Q_z \sin \frac{\pi}{L/R} \xi \sin \frac{\pi}{b/R} \theta$, where $Q_z = 1 Pa$. Table 2 presents the transverse displacement $\bar{w} = w \times 10^{10}$ at the middle position of the shell with respect to various values of R/h and η . The results are then validated against those calculated by the 3D theory of elasticity [44], the FSDT and the layer wise theory LW4 given in [29].

Table 2

The transverse displacement $\bar{w} = w \times 10^{10}$ of the FGM cylindrical shell at the middle position.

R/h	Elastic 3D [44]	Present $K=3$	Present $K=2$	FSDT [29]	LW4 [29]
$\eta = 1$					
100	5.2783	5.2782	4.4163	4.3735	5.2783

10	0.0170	0.0173	0.0159	0.0170	0.0170
4	0.0019	0.0016	0.0031	0.0054	0.0013
$\eta = 4$					
100	7.9738	7.9711	6.6315	6.5603	7.9734
10	0.0314	0.0328	0.0269	0.0277	0.0315
4	0.0032	0.0040	0.0051	0.0090	0.0022
$\eta = 10$					
100	9.2029	9.2014	7.6154	7.5561	9.2033
10	0.0404	0.0430	0.0337	0.0358	0.0405
4	0.0042	0.0064	0.0077	0.0121	0.0022

It is seen in Table 2 that for short cylindrical shells, the model with $K=3$ may provide results close to the 3D theory of elasticity and the Layer Wise Theory LW4 model whereas the model with $K=2$ shows the results similar to those from the FSDT, and this kind of model is applicable to thin shells.

The third validation analysis is conducted for an FGM cylindrical shell with the two simply-supported edges. The material parameters are the same as those in the second validation analysis. The geometric parameters are as follows: the radius $R = 10m$, the length $L = 1m$, the relative thickness $R/h = 4$. The shell is subjected to a harmonic transverse normal load distributed on the outer surface $q^+ = Q_z \sin \frac{\pi}{L/R} \xi \sin \theta$, where $Q_z = 1 Pa$. The non-dimensional stresses and displacements calculated by the theoretical model with $K=3$ are shown in Table 3 and compared with the results from the 3D theory of elasticity [44]. Herein, ξ_0 is used to denote L/R .

The non-dimensional form of stresses and displacements are defined as [44]

$$\{\bar{u}, \bar{v}, \bar{w}\} = \frac{10^4 E_m \{u, v, w\}}{Q_z h (R/h)^4}, \quad \{\bar{\sigma}_\xi, \bar{\sigma}_\theta, \bar{\tau}_{\xi\theta}\} = \frac{10^2 \{\sigma_\xi, \sigma_\theta, \tau_{\xi\theta}\}}{Q_z (R/h)^2},$$

$$\{\bar{\tau}_{\xi z}, \bar{\tau}_{\theta z}\} = \frac{10^2 \{\tau_{\xi z}, \tau_{\theta z}\}}{Q_z (R/h)}, \quad \bar{\sigma}_z = \frac{\sigma_z}{Q_z}.$$

Table 3

The non-dimensional displacements and the stresses of the FGM cylindrical shell.

	\bar{u}	\bar{v}	\bar{w}	$\bar{\sigma}_\xi$	$\bar{\sigma}_\theta$	$\bar{\tau}_{\xi\theta}$	$\bar{\sigma}_z$	$\bar{\tau}_{\xi z}$	$\bar{\tau}_{\theta z}$
(ξ, θ)	$\left(0, \frac{\pi}{2}\right)$	$\left(\frac{\xi_0}{2}, 0\right)$	$\left(\frac{\xi_0}{2}, \frac{\pi}{2}\right)$	$\left(\frac{\xi_0}{2}, \frac{\pi}{2}\right)$	$\left(\frac{\xi_0}{2}, \frac{\pi}{2}\right)$	$(0, 0)$	$\left(\frac{\xi_0}{2}, \frac{\pi}{2}\right)$	$\left(0, \frac{\pi}{2}\right)$	$\left(\frac{\xi_0}{2}, 0\right)$
$\eta = 0.5$									
$z = -h/2$									
$K = 2$	65.516	200.22	334.46	-3.7783	5.4396	6.9982	0	0	0
$K = 3$	66.713	202.00	334.97	-3.0645	6.1713	7.0701	0	0	0
Ref. [44]	66.732	201.99	334.97	-3.0504	6.2079	7.0941	0	0	0
$z = 0$									
$K = 2$	4.0474	182.72	327.81	7.0616	25.579	17.794	0.3818	8.3811	2.6468
$K = 3$	4.0435	184.10	330.64	7.6526	26.346	17.926	0.4020	7.5897	2.1443
Ref. [44]	4.0633	184.09	330.64	7.6328	26.308	17.904	0.4019	7.5923	2.1460
$z = h/2$									
$K = 2$	-57.09	165.83	321.15	35.320	43.073	16.791	1.0000	0	0
$K = 3$	-57.66	166.96	322.91	32.971	40.678	16.882	1.0000	0	0
Ref. [44]	-57.655	166.94	322.91	32.897	40.593	16.885	1,0000	0	0
$\eta = 1$									
$z = -h/2$									
$K = 2$	87.131	245.89	413.13	-4.5131	5.5786	7.4716	0	0	0
$K = 3$	88.802	248.16	413.14	-3.6376	6.4579	7.5530	0	0	0
Ref. [44]	88.819	248.13	413.13	-3.6717	6.4938	7.6111	0	0	0
$z = 0$									
$K = 2$	11.493	224.18	404.71	5.0891	24.047	17.358	0.3196	7.8095	2.4716
$K = 3$	11.526	225.94	408.23	5.8924	25.024	17.491	0.3395	7.0152	1.9720
Ref. [44]	11.559	225.91	408.20	5.8800	24.973	17.451	0,3394	7.0175	1.9735
$z = h/2$									
$K = 2$	-64.220	203.09	396.30	40.816	52.164	20.966	1.0000	0	0
$K = 3$	-64.864	204.53	398.70	37.918	49.252	21.089	1.0000	0	0
Ref. [44]	-64.861	204.49	398.68	37.792	49.105	21.079	1.0000	0	0
$\eta = 2$									
$z = -h/2$									
$K = 2$	119.01	316.69	534.80	-6.3629	7.0586	9.7424	0	0	0
$K = 3$	121.34	319.90	534.30	-5.0490	8.3581	9.8570	0	0	0
Ref. [44]	121.31	319.84	534.34	-5.1432	8.2629	9.8622	0	0	0

$z = 0$									
$K = 2$	21.993	288.66	523.71	3.1089	20.125	15.004	0.2706	7.4707	2.3568
$K = 3$	22.052	291.16	528.62	4.0199	21.195	15.130	0.2907	6.6427	1.8423
Ref. [44]	22.185	291.15	528.56	4.0474	21.174	15.082	0.2906	6.6434	1.8443
$z = h/2$									
$K = 2$	-75.967	261.19	512.61	49.628	66.308	27.436	1.0000	0	0
$K = 3$	-76.756	263.28	516.37	45.903	62.638	27.626	1.0000	0	0
Ref. [44]	-76.749	263.23	516.36	45.593	62.278	27.575	1.0000	0	0

Analyzing the data in Table 3, it is found that for shells of medium and large length, results from the model with $K=3$ are very close to those from the 3D theory of elasticity, while the model with $K=2$ also can guarantee an acceptable level of accuracy.

The above three analyses may confirm the validity of the model used in the present study. The model with $K=3$ provides results that are in good agreement with the 3D theory of elasticity for all cases. The model with $K=2$ is used in the calculation of shells of small to medium thickness and medium to large length.

4.2. The effect of the boundary condition

The shell with the following parameters is used to study the effect of the boundary condition: radius $R = 1m$, the outer surface is made of Aluminum Alloy Al2024 with $\mu_m = 0.3$ and $E_m = 73GPa$, the inner surface is made of ceramic (Alumina Al_2O_3) with $\mu_c = 0.3$ and $E_c = 380GPa$, the power-law index $\eta = 1$, the length L and the relative thickness R/h are variable. The shell is subjected to a transverse normal load distributed uniformly on the outer surface $q^+ = Q_z$, where $Q_z = 1 Pa$. The following boundary conditions are investigated: clamped support - clamped support (C-C), clamped support - simple support (C-S), simple support - simple support (S-S), clamped support - free (C-F). The non-dimensional stresses and transverse displacement are defined as



$$\bar{w} = \frac{10^4 E_m w}{Q_z h (R/h)^4}, \left\{ \bar{\sigma}_\xi, \bar{\sigma}_\theta, \bar{\tau}_{\xi\theta}, \bar{\tau}_{\xi z}, \bar{\tau}_{\theta z}, \bar{\sigma}_z \right\} = \frac{\left\{ \sigma_\xi, \sigma_\theta, \tau_{\xi\theta}, \tau_{\xi z}, \tau_{\theta z}, \sigma_z \right\}}{Q_z}. \quad (28)$$

Table 4 shows the non-dimensional transverse displacement \bar{w} and the stresses $\bar{\sigma}_\xi$, $\bar{\sigma}_\theta$,

$\bar{\tau}_{\xi z}$, $\bar{\sigma}_z$ at the middle position and the edge $\xi = \xi_0$ obtained by the use of the model with $K=3$.

Table 4

The effect of the boundary condition on the non-dimensional of transverse displacement \bar{w} and the stresses $\bar{\sigma}_\xi$, $\bar{\sigma}_\theta$, $\bar{\tau}_{\xi z}$, $\bar{\sigma}_z$.

	\bar{w}	$\bar{\sigma}_\xi$	$\bar{\sigma}_\theta$	$\bar{\tau}_{\xi z}$	$\bar{\sigma}_z$	$\bar{\sigma}_\xi$	$\bar{\sigma}_\theta$	$\bar{\tau}_{\xi z}$	$\bar{\sigma}_z$
	$\left(\frac{\xi_0}{2}, 0\right)$ (0)	$\left(\frac{\xi_0}{2}, 0\right)$ $(\pm h/2)$	$\left(\frac{\xi_0}{2}, 0\right)$ $(\pm h/2)$	$\left(\frac{\xi_0}{2}, 0\right)$ $(\pm 3h/8)$	$\left(\frac{\xi_0}{2}, 0\right)$ $(\pm h/4)$	$(\xi_0, 0)$ $(\pm h/2)$	$(\xi_0, 0)$ $(\pm h/2)$	$(\xi_0, 0)$ $(\pm 3h/8)$	$(\xi_0, 0)$ $(\pm h/4)$
$L = 4R, R/h = 10$									
C-C	29.777	1.093		0.000		-8.522	-3.652	-4.010	-6.430
		4.758	17.972	0.000	0.411	39.236	16.816	-7.706	11.454
C-S	32.713	0.116	3.319	0.000	0.901	0.000	0.000	-0.944	-0.339
		-0.329	17.975	0.000	0.411	0.000	0.000	-1.149	0.496
S-S	32.718	0.115	3.319	0.000	0.901	0.000	0.000	-0.944	-0.339
		-0.327	17.978	0.000	0.411	0.000	0.000	-1.149	0.496
C-F	32.710	0.114	3.319	0.000	0.901	0.000	3.325	0.000	0.906
		-0.325	17.974	0.000	0.411	0.000	18.310	0.000	0.433
$L = 0.5R, R/h = 10$									
C-C	7.904	2.691	1.727	0.000	0.891	-7.169	-3.073	-3.596	-4.880
		-7.671	1.799	0.000	0.230	26.536	11.373	-5.825	7.126
C-S	12.177	3.253	2.289	0.156	0.883	0.000	0.000	-1.060	-0.339
		-11.560	2.973	0.377	0.237	0.000	0.000	-1.436	0.496
S-S	19.571	4.597	3.365	0.000	0.868	0.000	0.000	-1.095	-0.339
		-16.076	5.717	0.000	0.258	0.000	0.000	-1.516	0.496
C-F	19.113	0.249	2.082	0.084	0.905	0.000	4.023	0.000	0.887
		-1.039	10.128	0.191	0.329	0.000	22.482	0.000	0.535
$L = 4R, R/h = 100$									
C-C	0.294	9.549	32.295	0.000	0.880	-83.189	-35.652	-29.581	-67.558
		48.863	168.939	0.000	0.380	362.686	155.437	-57.182	114.115

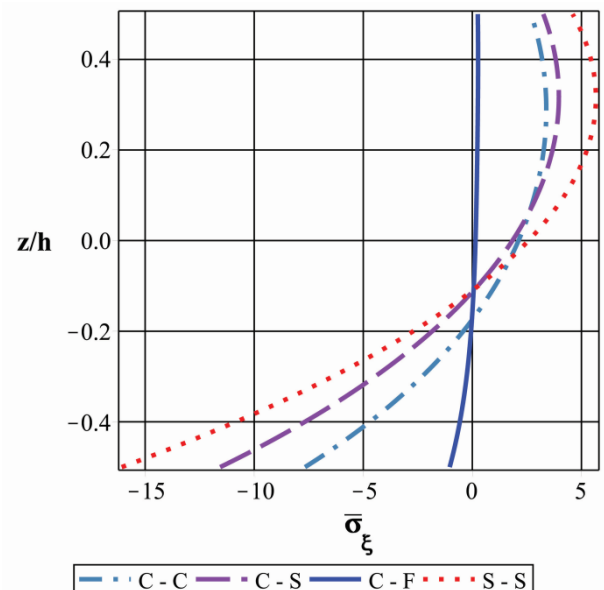
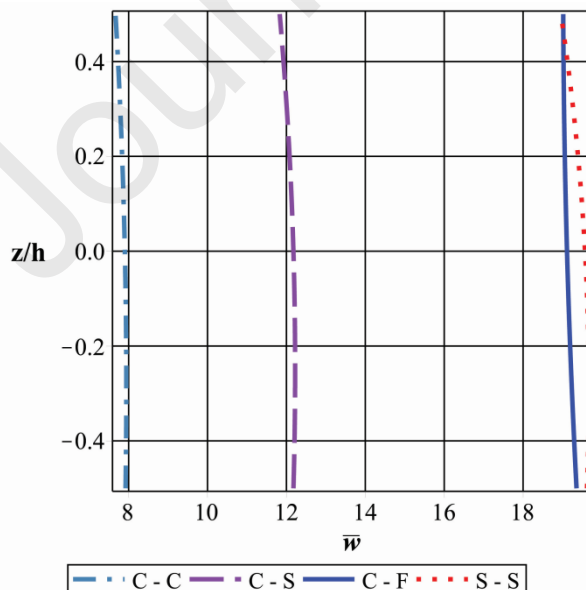
C-S	0.323	0.100	32.295	0.000	0.880	0.000	0.000	-1.935	-0.325
		-0.323	168.939	0.000	0.380	0.000	0.000	-3.465	0.469
S-S	0.323	0.100	32.295	0.000	0.880	0.000	0.000	-1.935	-0.325
		-0.323	168.939	0.000	0.380	0.000	0.000	-3.465	0.469
C-F	0.323	0.100	32.295	0.000	0.880	0.000	32.306	0.000	0.880
		-0.323	168.939	0.000	0.380	0.000	169.250	0.000	0.383

Figures 2 and 3 show the distributions of the non-dimensional transverse displacement \bar{w} and the stresses $\bar{\sigma}_\xi$, $\bar{\sigma}_\theta$, $\bar{\sigma}_z$ along the thickness direction at various positions for shells of several values of length and at different boundary conditions. From these data, it is possible to state that

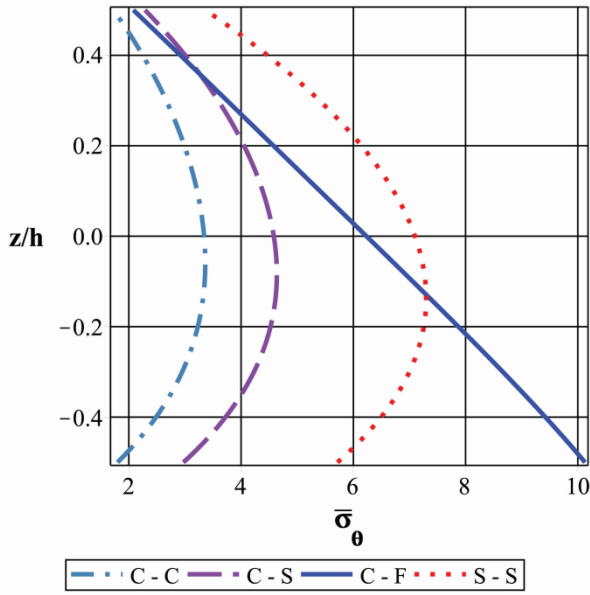
- For shells of medium or large length, at the middle position (large distances from the edges), the boundary condition does not have any substantial effect on the displacements and the stresses.

- At the edges of the shell, the maximum stress depends on the boundary condition. The stress concentration occurs at the clamped edge, and the transverse normal stress $\bar{\sigma}_z$ increases considerably and reaches 30% of the maximum value.

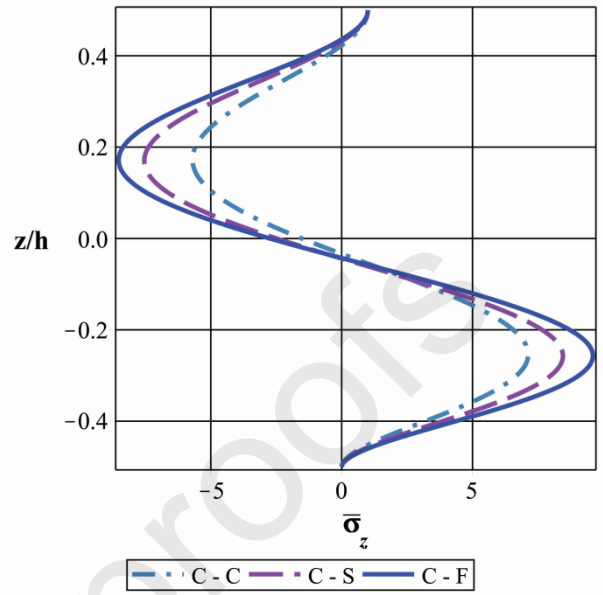
- For short shells, the boundary condition has a large effect on the displacements and the stress components in the whole structure.



a) Variation of non-dimensional displacement \bar{w} at the middle position $\xi = \xi_0 / 2$



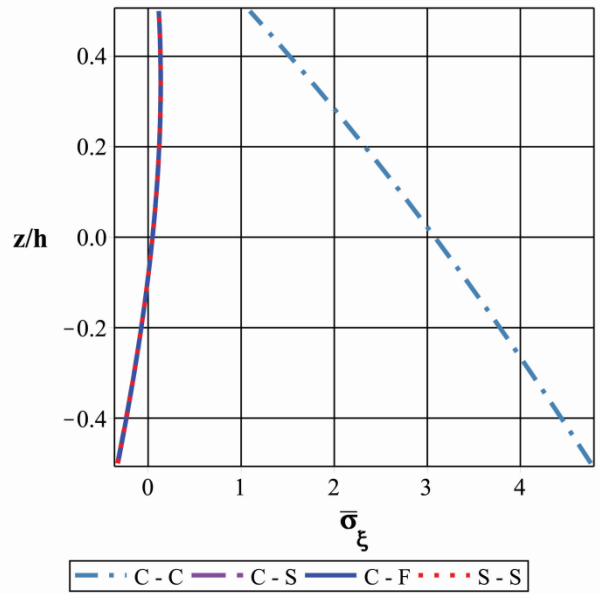
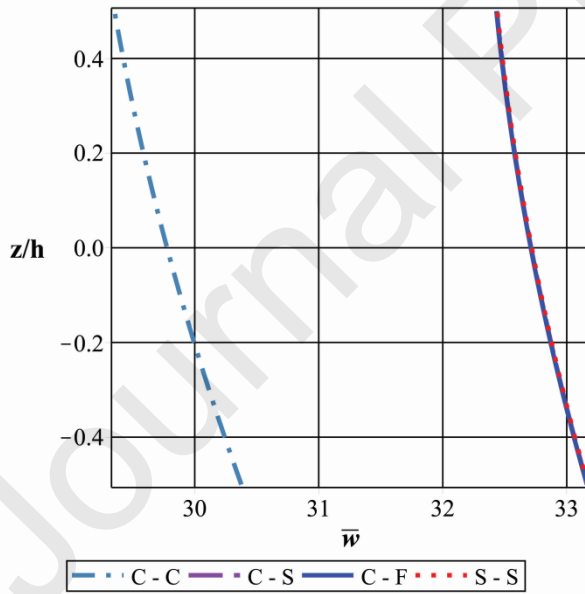
b) Variation of non-dimensional stress $\bar{\sigma}_\xi$ at the middle position $\xi = \xi_0 / 2$



c) Variation of non-dimensional stress $\bar{\sigma}_\theta$ at the middle position $\xi = \xi_0 / 2$

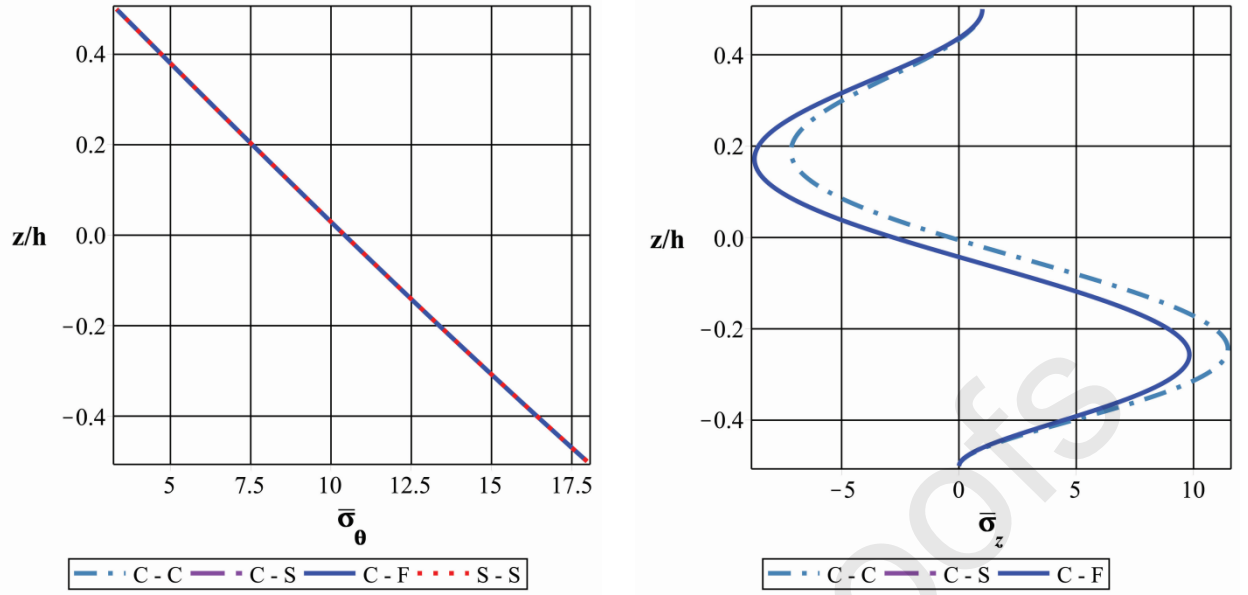
d) Variation of non-dimensional stress $\bar{\sigma}_z$ at the boundary position $\xi = 0$

Fig. 2. Variation of non-dimensional displacement and the stresses through the thickness z/h for $L = 0.5R$, $R/h = 10$, $\eta = 1$.



a) Variation of non-dimensional displacement \bar{w} at the middle position $\xi = \xi_0 / 2$

b) Variation of non-dimensional stress $\bar{\sigma}_\xi$ at the middle position $\xi = \xi_0 / 2$



c) Variation of non-dimensional stress $\bar{\sigma}_\theta$ at the middle position $\xi = \xi_0 / 2$

d) Variation of non-dimensional stress $\bar{\sigma}_z$ at the boundary position $\xi = 0$

Fig. 3. Variation of non-dimensional displacement and the stresses through the thickness z/h for $L = 4R$, $R/h = 10$, $\eta = 1$.

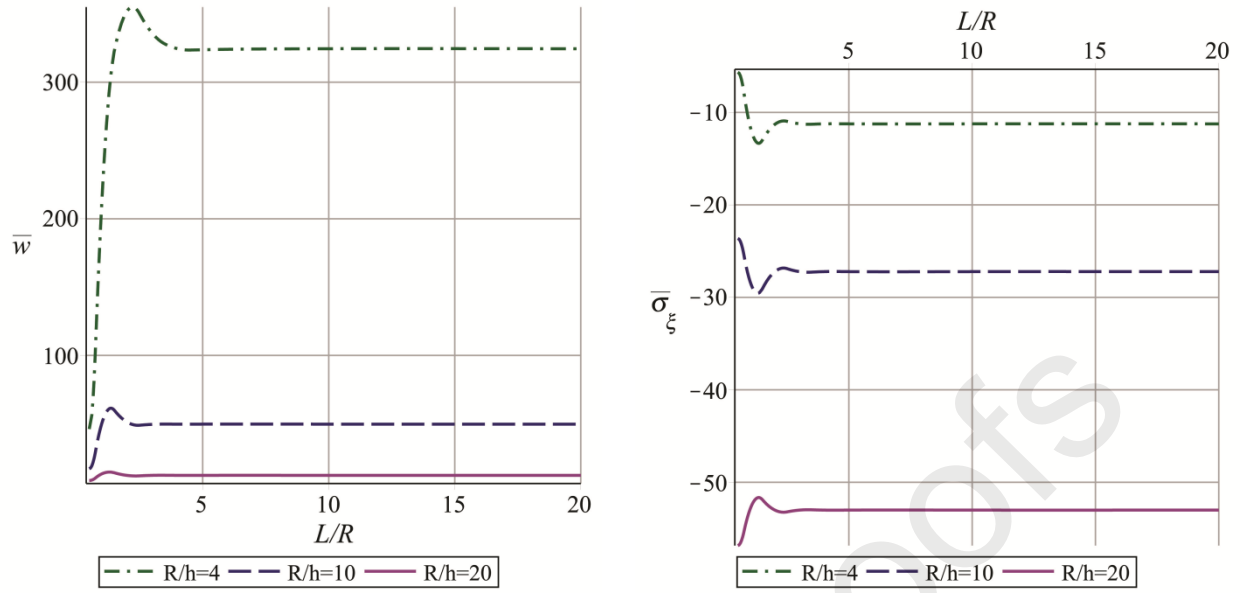
4.3. The effects of thickness and length

We investigate a shell with the following parameters: the radius $R = 1m$, the inner surface is made of Aluminum Alloy Al2024 with $\mu_m = 0.3$ and $E_m = 73GPa$, the outer surface is made of ceramic Zirconia with $\mu_c = 0.3$ and $E_c = 168.06 GPa$, the power-law index $\eta = 0.2$, the length L and the relative thickness R/h are variable. The boundary condition is clamped support - simple support (C-S). The shell is subjected to a transverse normal load distributed uniformly on the outer surface $q^+ = Q_z$, where $Q_z = 1 Pa$. Table 5 presents the non-dimensional transverse displacement \bar{w} and the stresses $\bar{\sigma}_\xi$, $\bar{\sigma}_\theta$, $\bar{\sigma}_z$ calculated by equation (28) at the middle position and the edge $\xi = 0$ using the theoretical model with $K=3$. It is seen that, for shells of small length, the thickness and the length have large influences on the displacement field and the stresses. For shells of large length ($L/R \geq 4$), we can observe only the effect of the thickness while the that of the length is negligible. This trend is exhibited clearly in Fig. 4.

Table 5

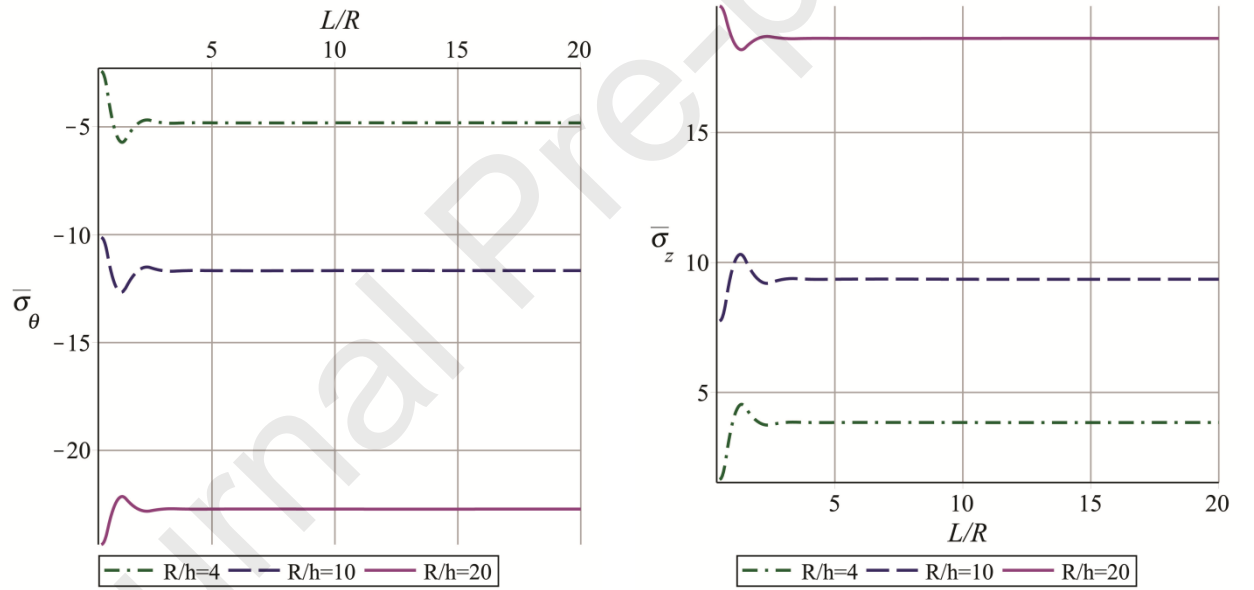
The effects of thickness and length on the non-dimensional transverse displacement \bar{w} and the stresses $\bar{\sigma}_\xi$, $\bar{\sigma}_\theta$, $\bar{\sigma}_z$.

	\bar{w}	$\bar{\sigma}_\xi$	$\bar{\sigma}_\theta$	$\bar{\sigma}_z$	$\bar{\sigma}_\xi$	$\bar{\sigma}_\theta$	$\bar{\sigma}_z$
R/h	$\left(\frac{\xi}{2}, 0, 0\right)$	$\left(\frac{\xi}{2}, 0, -\frac{h}{2}\right)$	$\left(\frac{\xi_0}{2}, 0, -\frac{h}{2}\right)$	$\left(\frac{\xi}{2}, 0, -\frac{h}{4}\right)$	$\left(0, 0, -\frac{h}{2}\right)$	$\left(0, 0, -\frac{h}{2}\right)$	$\left(0, 0, -\frac{h}{4}\right)$
$L = 0.5R$							
4	46.1308	-1.4464	-0.0553	0.1557	3.1512	1.3462	1.6483
10	17.0310	-5.2476	0.7597	0.1398	15.0752	6.4608	7.7488
20	8.4325	-11.3291	5.8366	0.1603	36.9279	15.8262	19.8642
50	2.0455	-13.6230	30.5323	0.2072	85.5064	36.6456	47.5249
100	0.5204	-3.8802	68.9029	0.2245	163.8853	70.2365	92.4781
$L = 4R$							
4	324.5210	0.1075	3.3387	0.2902	7.1825	3.0782	3.8415
10	49.6960	0.0219	7.1147	0.2449	17.4940	7.5403	9.3541
20	12.2132	0.0215	13.5152	0.2315	34.4170	14.7502	18.6219
50	1.9327	0.0167	32.7477	0.2236	83.6725	35.8597	46.4488
100	0.4814	0.0152	64.8153	0.2211	164.4653	70.4851	92.8063
$L = 10R$							
4	324.4943	0.0534	3.3202	0.2890	7.1821	3.0781	3.8408
10	49.7008	0.0286	7.1175	0.2450	17.5940	7.5403	9.3541
20	12.2132	0.0210	13.5150	0.2315	34.4170	14.7502	18.6219
50	1.9327	0.0167	32.7477	0.2236	83.6725	35.8597	46.4488
100	0.4814	0.0152	64.8153	0.2211	164.4653	70.4851	92.8063



a) Variation of non-dimensional displacement \bar{w} at the middle position $\xi = \xi_0 / 2, z = 0$

b) Variation of non-dimensional stress $\bar{\sigma}_\xi$ at the boundary position $\xi = 0, z = h / 2$



c) Variation of non-dimensional stress $\bar{\sigma}_\theta$ at the boundary position $\xi = 0, z = h / 2$

d) Variation of non-dimensional stress $\bar{\sigma}_z$ at the boundary position $\xi = 0, z = -h / 4$

Fig. 4. Variation of non-dimensional displacement and the stresses with relative length L/R for different relative thickness.

4.4. The effect of power-law index

The cylindrical shell with the following parameters are investigated: the radius $R = 1m$, the inner surface is made of Aluminum Alloy Al2024 with $\mu_m = 0.3$ and $E_m = 73GPa$, the outer surface is made of ceramic Alumina Al_2O_3 with $\mu_c = 0.3$ and $E_c = 380GPa$, the length L and the relative thickness R/h are variable. The boundary condition is clamped support - free (C-F).

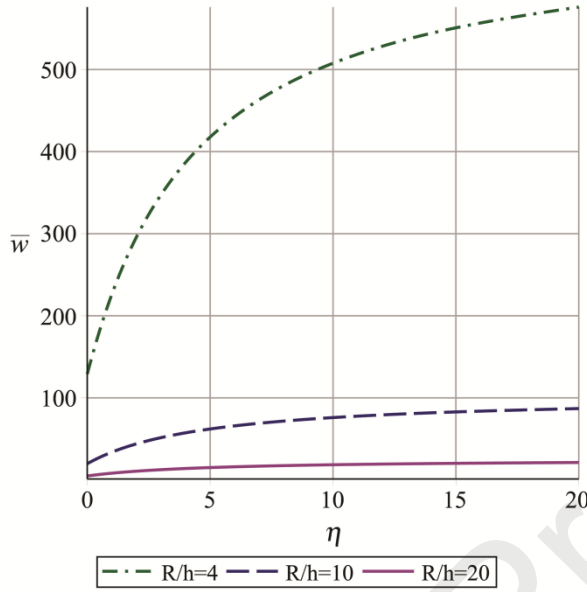
The shell is subjected to a transverse normal load distributed linearly on the outer surface $q^+ = Q_z(\xi_0 - \xi)$, where $Q_z = 1 Pa$. Table 6 presents the non-dimensional transverse displacement \bar{w} and the stresses $\bar{\sigma}_\xi$, $\bar{\sigma}_\theta$, $\bar{\sigma}_z$ calculated by equation (28) at the middle position and the edge $\xi = 0$ using the theoretical model with $K=3$. Figure 5 shows the variation of non-dimensional transverse displacement \bar{w} and the stresses $\bar{\sigma}_\xi$, $\bar{\sigma}_\theta$, $\bar{\sigma}_z$ against the power-law index η for various relative thickness R/h . It is found that the absolute values of the non-dimensional stresses $\bar{\sigma}_\xi$, $\bar{\sigma}_\theta$ and the non-dimensional transverse displacement \bar{w} increase with the power-law index η . The non-dimensional stress $\bar{\sigma}_z$ reaches its minimum value when η is around 1.8. This finding is important as it demonstrates the effect of the inhomogeneity on the performance of FGM structures.

Table 6

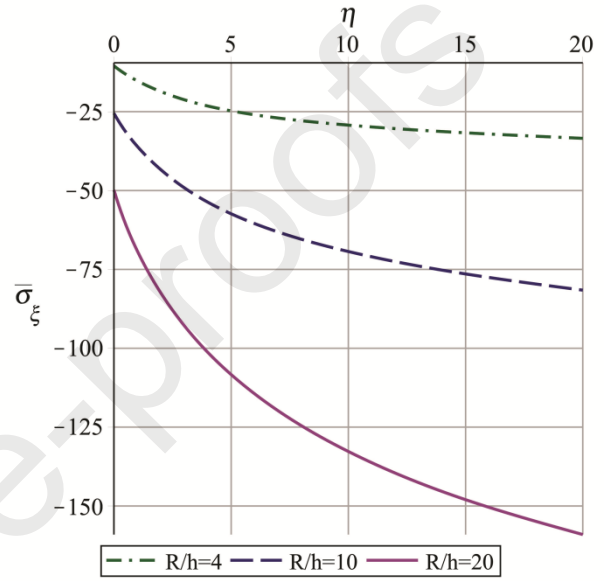
The effect of power-law index η and thickness on the non-dimensional transverse displacement \bar{w} and the stresses $\bar{\sigma}_\xi$, $\bar{\sigma}_\theta$, $\bar{\sigma}_z$.

	\bar{w}	$\bar{\sigma}_\xi$	$\bar{\sigma}_\theta$	$\bar{\sigma}_z$	$\bar{\sigma}_\xi$	$\bar{\sigma}_\theta$	$\bar{\sigma}_z$
η	$\left(\frac{\xi_0}{2}, 0, 0\right)$	$\left(\frac{\xi_0}{2}, 0, -\frac{h}{2}\right)$	$\left(\frac{\xi_0}{2}, 0, -\frac{h}{2}\right)$	$\left(\frac{\xi_0}{2}, 0, -\frac{h}{4}\right)$	$\left(0, 0, -\frac{h}{2}\right)$	$\left(0, 0, -\frac{h}{2}\right)$	$\left(0, 0, -\frac{h}{4}\right)$
$R/h = 4$							
0	129.0714	0.0957	5.1385	0.3286	10.4056	4.4596	3.9252
0.1	140.2744	0.0795	3.4006	0.2971	7.2584	3.1108	3.8544
0.2	151.1466	0.0669	2.4274	0.2704	5.4194	2.3226	3.7856
1	226.1590	0.0854	1.7570	0.1697	4.4816	1.9207	3.3709
10	507.6642	0.2471	3.9957	0.2536	9.1825	3.9354	3.7303
$R/h = 20$							
0	4.8838	0.0101	21.0224	0.2643	49.8812	21.3777	19.2160
0.1	5.2778	0.0182	13.8048	0.2376	34.7574	14.8960	18.7178
0.2	5.6583	0.0203	9.7871	0.2152	25.9384	11.1165	18.2595
1	8.2678	0.0429	6.8540	0.1312	21.8030	9.3441	15.8677
10	18.5590	0.1536	15.4408	0.1938	43.2432	18.5328	18.4692
$R/h = 100$							

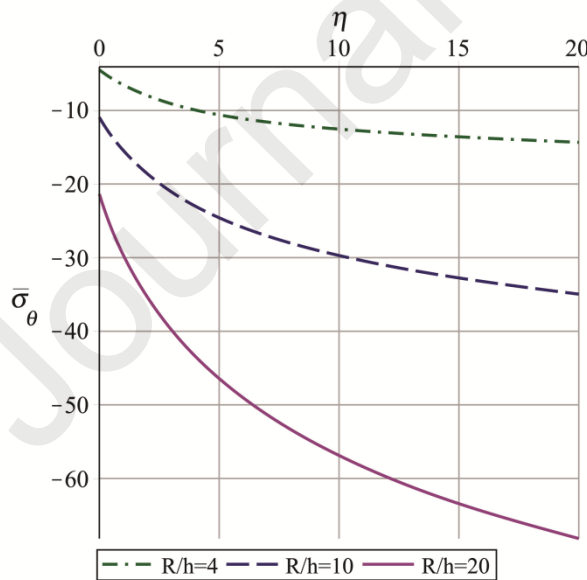
0	0.1928	0.0019	101.0044	0.2528	237.5102	101.7901	95.9692
0.1	0.2081	0.0122	66.2309	0.2270	165.9082	71.1035	93.3165
0.2	0.2228	0.0156	46.8951	0.2054	124.1057	53.1881	90.8971
1	0.3240	0.0382	32.6278	0.1246	106.3988	45.5995	78.5827
10	0.7273	0.1426	73.2942	0.1834	204.5827	87.6782	92.7428



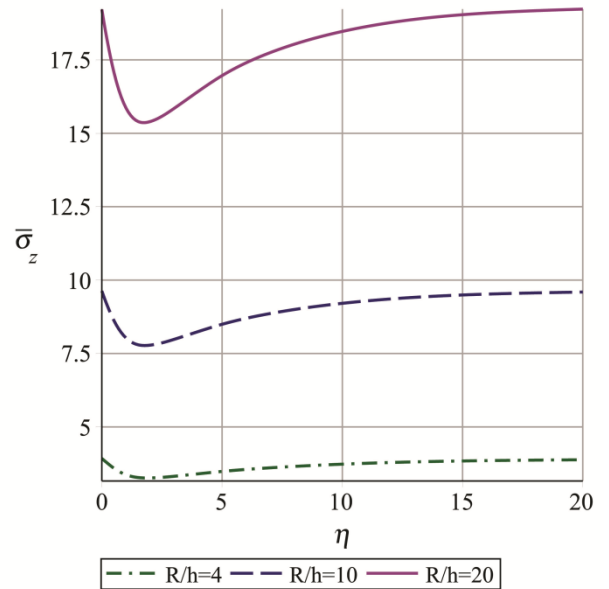
a) Variation of non-dimensional displacement \bar{w} at the middle position $\xi = \xi_0 / 2, z = 0$



b) Variation of non-dimensional stress $\bar{\sigma}_\xi$ at the boundary position $\xi = 0, z = h / 2$



c) Variation of non-dimensional stress $\bar{\sigma}_\theta$ at the boundary position $\xi = 0, z = h / 2$



d) Variation of non-dimensional stress $\bar{\sigma}_z$ at the boundary position $\xi = 0, z = -h / 4$

Fig. 5. Variation of non-dimensional displacement and the stresses with power-law index η for

various relative thickness values R/h .

4.5. Stress concentration analysis

As shown above, stress concentration mainly occurs near a clamped edge. Hence, in the present subsection, we focus on this phenomenon for this kind of boundary condition using theoretical models with $K=3$ and $K=2$, and the FSDT. The input parameters are as follows: the radius $R=1m$, the inner surface is made of Aluminum Alloy Al2024 with $\mu_m=0.3$ and $E_m=73GPa$ while the outer surface is made of ceramic Alumina Al_2O_3 with $\mu_c=0.3$ and $E_c=380GPa$, the length $L=4$. The shell is clamped at the two edges and subjected to a transverse normal load distributed uniformly on a part of the outer surface as

$$q^+ = \begin{cases} 0, & \text{for } \xi_0/2 < \xi \leq \xi_0, \\ Q_z(\xi), & \text{for } 0 \leq \xi \leq \xi_0/2, \quad Q_z(\xi) = 1Pa. \end{cases}$$

The load applied on the shell is illustrated in Fig. 6. The non-dimensional normal stresses $\bar{\sigma}_\xi$, $\bar{\sigma}_\theta$, $\bar{\sigma}_z$ are determined by equation (28) at a clamped edge with several values of the power-law index η and the relative thickness R/h as shown in Figs. 7-9.

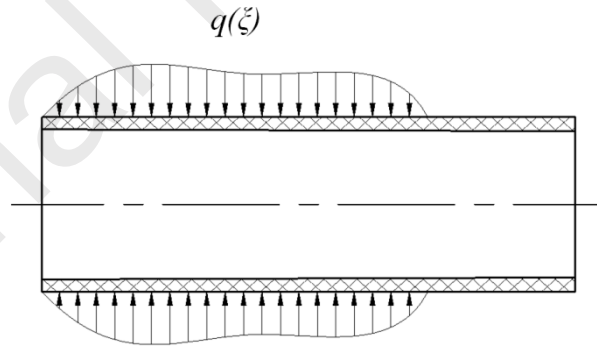


Fig. 6. Model of transverse normal local load tác dụng lên vỏ.

Analyzing the results, it is found that

- At a clamped edge, the stresses increase considerably, the stress concentration phenomenon is seen in both thick and thin shells.
- The normal transverse stress $\bar{\sigma}_z$ must be included while investigating structures with a clamped-support boundary condition due to the existence of stress concentration.

- The size of the stress concentration zone is small, and does not exceed half of the thickness.

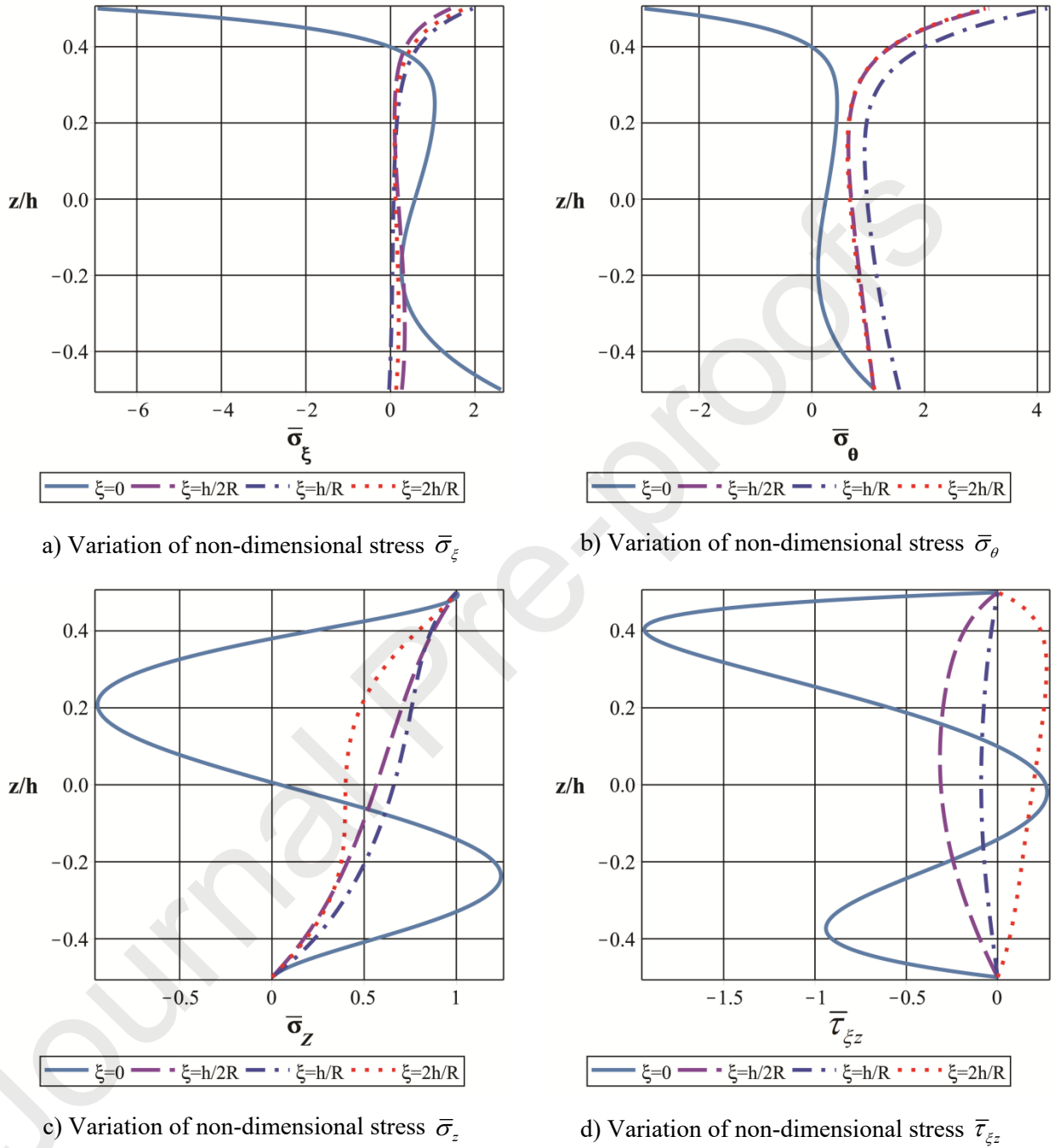


Fig. 7. Variation of non-dimensional stresses through the thickness z/h at the boundary zone for $L = 4R$, $R/h = 10$, $\eta = 10$.

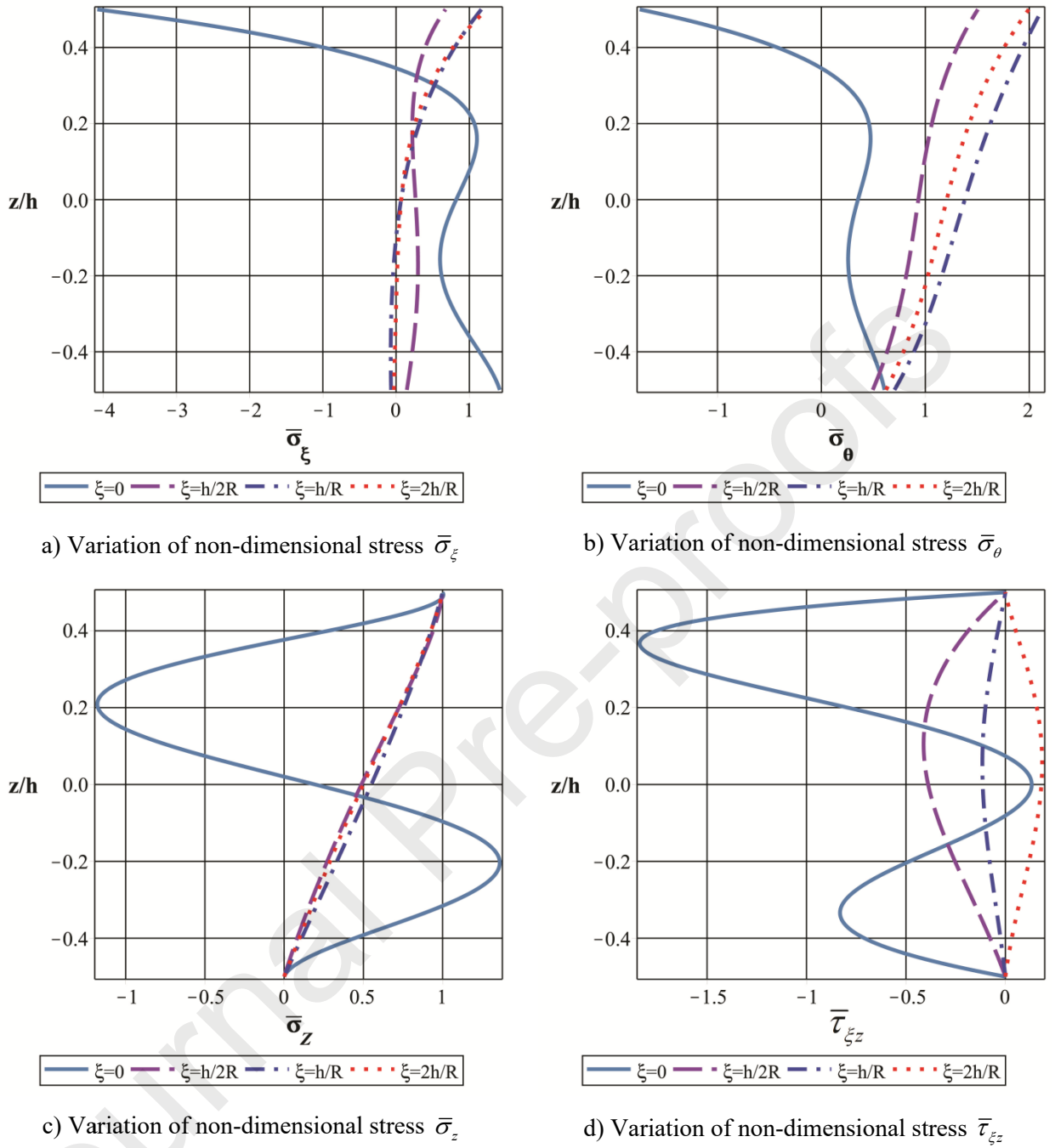


Fig. 8. Variation of non-dimensional stresses through the thickness z/h at the boundary zone for $L = 4R$, $R/h = 30$, $\eta = 1$.

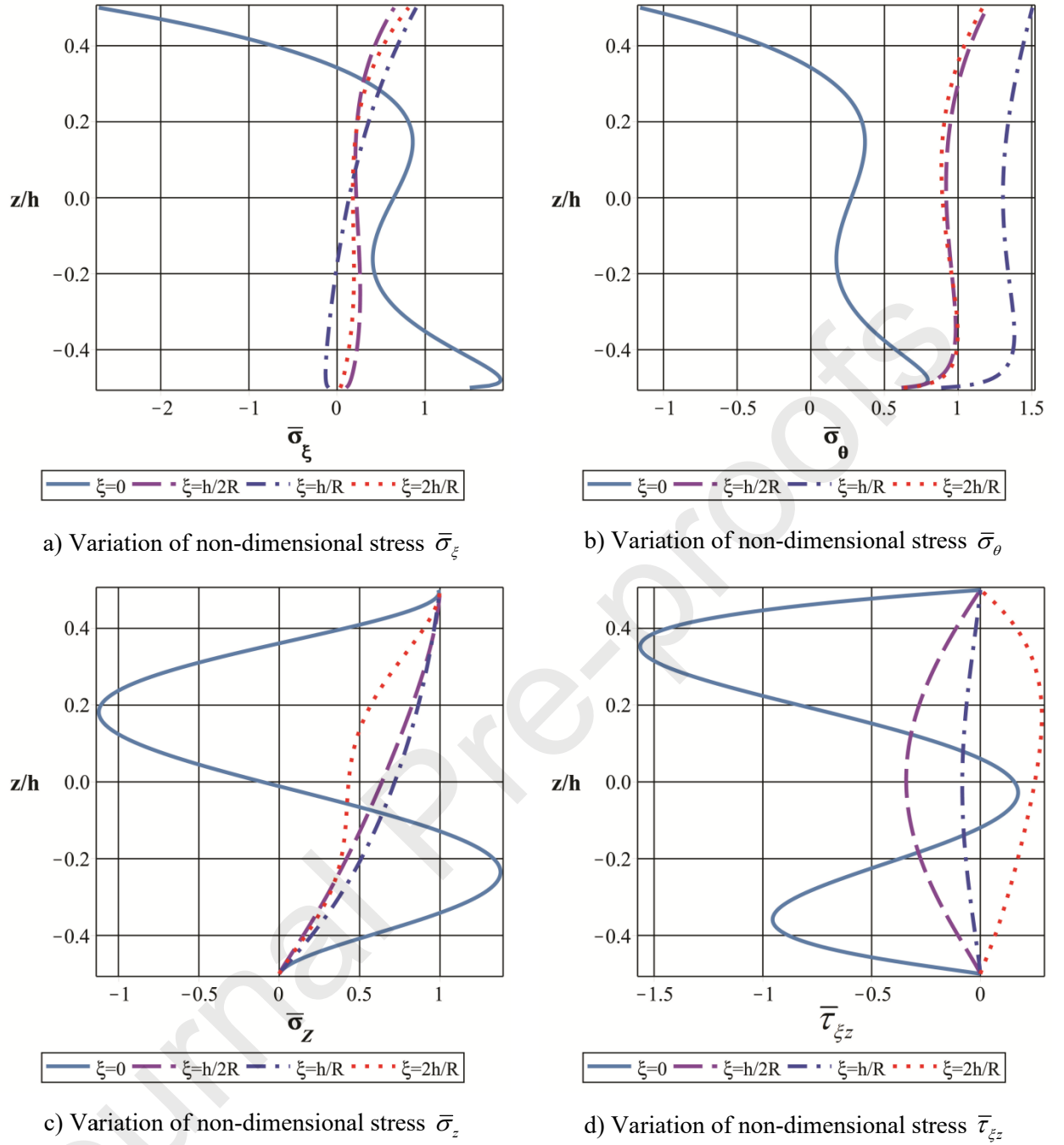


Fig. 9. Variation of non-dimensional stresses through the thickness z/h at the boundary zone for $L = 4R$, $R/h = 100$, $\eta = 0.2$.

5. Conclusions

On the basis of the calculation results presented in this paper, we can come to the following principle conclusions:

1. The governing equations for the calculation of FGM cylindrical shells have been established based on the quasi-3D type HSDT, which includes the effects of transverse shear and normal deformations. The material distribution along the thickness of the shell is assumed to

follow a power law. The fundamental and the boundary conditions are derived using the virtual work principle. The solution from the equilibrium equations is derived through the use of simple trigonometric series and the Laplace transform. The obtained results in this study are compared with those by other authors for several cases, and the validity of the calculation model is ascertained.

2. Analyses were conducted to study the effects of the boundary condition, the relative thickness R/h , the relative length L/R , the power-law index of shells on the nondimensional displacements and the stresses. The results show that the boundary condition, the power-law index and several geometric parameters have great effects on the displacements and the stresses.

3. The stress concentration effect was found and analyzed at the clamped-edge zone. The paper has shown the effects of the relative thickness and the power-law index on the distribution of stresses in this zone.

References

- [1] Koizumi M. FGM activities in Japan. *Composites Part B: Engineering* 1997;28(1):1-4.
- [2] Jha DK, Kant T, Singh RK. A critical review of recent research on functionally graded plates. *Composite Structures* 2013;96:833-849.
- [3] Birman V, Byrd LW. Modeling and analysis of functionally graded materials and structures. *Applied Mechanics Reviews* 2007;60(5):195-216.
- [4] Thai HT, Kim SE. A review of theories for the modeling and analysis of functionally graded plates and shells. *Composite Structures* 2015;128:70-86.
- [5] Reddy JN. *Mechanics of laminated composite plates and shells – theory and analysis*. Boca Raton: CRC Press 2004.
- [6] Kirchhoff VG. *Über das gleichgewicht und die bewegung einer elastischen scheibe*. *Journal Fur Die Reine und Angewandte Mathematik* 1850;40:51-88.
- [7] Woo J, Meguid SA. Nonlinear analysis of functionally graded plates and shallow shells. *International Journal of Solids and Structures* 2001;38(42):7409-7421.
- [8] Nguyen DD. Nonlinear dynamic response of imperfect eccentrically stiffened FGM double curved shallow shells on elastic foundation. *Composite Structures* 2013;99:88-96.
- [9] Dai HL, Dai T. Analysis for the thermoelastic bending of a functionally graded material cylindrical shell. *Meccanica* 2014;49:1069-81.
- [10] Pradhan SC, Loy CT, Lam KY, Reddy JN. Vibration characteristics of functionally graded cylindrical shells under various boundary conditions. *Applied Acoustics* 2000;61(1):111-129.

- [11] Alijani F, Amabili M, Karagiozis K, Bakhtiari-Nejad F. Nonlinear vibrations of functionally graded doubly curved shallow shells. *Journal of Sound and Vibration* 2011;330(7):1432-1454.
- [12] Du C, Li Y. Nonlinear resonance behavior of functionally graded cylindrical shells in thermal environments. *Composite Structures* 2013;102:164-174.
- [13] Shen HS. Postbuckling analysis of axially-loaded functionally graded cylindrical shells in thermal environments. *Composites Science and Technology* 2002;62(7–8):977-987.
- [14] Huang H, Han Q, Feng N, Fan X. Buckling of functionally graded cylindrical shells under combined loads. *Mechanics of Advanced Materials and Structures* 2011;18(5):337-346.
- [15] Sun J, Xu X, Lim CW. Buckling of functionally graded cylindrical shells under combined thermal and compressive loads. *Journal of Thermal Stresses* 2014;37(3):340-362.
- [16] Mindlin RD. Influence of rotatory inertia and shear on flexural motions of isotropic, elastic plates. *Journal of Applied Mechanics* 1951;18(1):31-38.
- [17] Zhao X, Liew KM. Geometrically nonlinear analysis of functionally graded shells. *Int J Mech Sci* 2009;51:131–44.
- [18] Arciniega RA, Reddy JN. Large deformation analysis of functionally graded shells. *Int J Solids Struct* 2007;44:2036–52.
- [19] Tornabene F, Ceruti A. Mixed static and dynamic optimization of four-parameter functionally graded completely doubly curved and degenerate shells and panels using GDQ method. *Mathematical Problems in Engineering* 2013;1:1-33.
- [20] Reddy JN, Chin CD. Thermomechanical analysis of functionally graded cylinders and plates. *Journal of Thermal Stresses* 1998;21(6):593-626.
- [21] Su Z, Jin G, Shi S, Ye T, Jia X. A unified solution for vibration analysis of functionally graded cylindrical, conical shells and annular plates with general boundary conditions. *Int J Mech Sci* 2014;80:62–80.
- [22] Chorf SM, Houmat A. Non-linear free vibration of a functionally graded doubly curved shallow shell of elliptical plan-form. *Composite Structures* 2010;92:2573–81.
- [23] Sheng GG, Wang X. Studies on dynamic behavior of functionally graded cylindrical shells with PZT layers under moving loads. *Journal of Sound and Vibration* 2009;323:772–89.
- [24] Khazaeinejad P, Najafizadeh MM, Jenabi J, Isvandzibaei MR. On the buckling of functionally graded cylindrical shells under combined external pressure and axial compression. *Journal of Pressure Vessel Technology* 2010;32(6):064501.
- [25] Sheng GG, Wang X. Thermal vibration, buckling and dynamic stability of functionally graded cylindrical shells embedded in an elastic medium. *Journal of Reinforced Plastics and Composites* 2007;27(2):117-134.
- [26] Reddy JN, Liu CF. A higher-order shear deformation theory of laminated elastic shells. *Int J Eng Sci* 1985;23(3):319-330.
- [27] Touratier M. A refined theory of laminated shallow shells. *Int J Solids Struct* 1992;29(11):1401-1415.

- [28] Ferreira AJM, Carrera E, Cinefra M, Roque CMC, Polit O. Analysis of laminated shells by a sinusoidal shear deformation theory and radial basis functions collocation, accounting for through-the-thickness deformations. *Composites Part B* 2011;42(5):1276-1284.
- [29] Carrera E, Brischetto S, Cinefra M and Soave M. Refined and Advanced Models for Multilayered Plates and Shells Embedding Functionally Graded Material Layers. *Mechanics of Advanced Materials and Structures* 2010;17(8):603-621.
- [30] Mantari JL, Guedes Soares C. Analysis of isotropic and multilayered plates and shells by using a generalized higher-order shear deformation theory. *Composite Structures* 2012;94(8):2640-2656.
- [31] Viola E, Tornabene F, Fantuzzi N. General higher-order shear deformation theories for the free vibration analysis of completely doubly-curved laminated shells and panels. *Composite Structures* 2013;95:639-666.
- [32] Naghdi PM. On the theory of thin elastic shells. *Q Appl Math* 1957;14:369-80.
- [33] Vasiliev VV, Lurie SA. To a problem of improvement of the theory of shallow shells. *Izv. RAN. Mekh-Tverd-Tela* 1990;6:139-46.
- [34] Firsanov VV, Doan TN. Investigation of the statics and free vibrations of cylindrical shells on the basis of a nonclassical theory. *Compos Mech Comput Appl Int J* 2015;6(2):135–66.
- [35] Firsanov VV, Doan TN. Natural Oscillations of General Shells Based on Nonclassical Theory. *Journal of Machinery Manufacture and Reliability* 2014;43(5):349–357.
- [36] Doan TN, et al. Analysis of stress concentration phenomenon of cylinder laminated shells using higher-order shear deformation Quasi-3D theory. *Composite Structures* 2020; 232:111526.
- [37] Neves AMA, Ferreira AJM, Carrera E, et al. Free vibration analysis of functionally graded shells by a higher-order shear deformation theory and radial basis functions collocation, accounting for through-the-thickness deformations. *Eur J Mech A/Solids* 2013;37:24–34.
- [38] Punera D, Kant T. Elastostatics of laminated and functionally graded sandwich cylindrical shells with two refined higher order models. *Compos Struct* 2017;182:505–23.
- [39] Punera D, Kant T. Free vibration of functionally graded open cylindrical shells based on several refined higher order displacement models. *Thin-Walled Struct* 2017;119:707–26.
- [40] Mantari JL, Guedes Soares C. Bending analysis of thick exponentially graded plates using a new trigonometric higher order shear deformation theory. *Compos Struct* 2012;94:1991-2000.
- [41] Neves AMA, Ferreira AJM, Carrera E, et al. A quasi-3D sinusoidal shear deformation theory for the static and free vibration analysis of functionally graded plates. *Compos Part B* 2012;43:711-25.
- [42] Ferreira AJM, Carrera E, Cinefra M, Roque CMC, Polit O. Analysis of laminated shells by a sinusoidal shear deformation theory and radial basis functions collocation, accounting for through-the-thickness deformations. *Compos Part B* 2011;42:1276-84.
- [43] Santos H, Soares CMM, Soares CAM, Reddy JN. A semi-analytical finite element model for the analysis of cylindrical shells made of functionally graded materials. *Composite Structures* 2009;91:427–432.

- [44] Brischetto S. A general exact elastic shell solution for bending analysis of functionally graded structures. *Composite Structures* 2017; doi: <http://dx.doi.org/10.1016/j.compstruct.2017.04.002>

Journal Pre-proofs